Summer 8-10-2016

A Hybrid Technique of Energy Harvesting from Mechanical Vibration and Ambient Illumination

M Shafiqur Rahman
University of New Orleans, New Orleans, mrahman3@uno.edu

A Hybrid Technique of Energy Harvesting from Mechanical Vibration and Ambient Illumination

A Thesis

Submitted to the Graduate Faculty of the
University of New Orleans
in partial fulfillment of the
requirements for the degree of

Master of Science
in
Engineering - Mechanical concentration

by

M Shafiqur Rahman

B.Sc., Islamic University of Technology, 2011

August, 2016

DEDICATION

To

My Parents

who brought me in this world and taught me never to lose hope and always try to the end without expecting anything for earning an honest living

and

My Fiancée

who always encourages me to listen to my mind to do things as I think is good and always keeps faith on me

ACKNOWLEDGMENT

First of all, I would like to express my sincere gratitude to my advisor, Dr. Uttam K Chakravarty, for the continuous support, motivation, and guidance for my Master's study and research. His sense of professionalism, enthusiasm, and immense knowledge helped me not only to accomplish the thesis but also to foster my skills on professional problem-analyzing, problem-solving, and report-writing.

Besides my advisor, I would like to thank the rest of my thesis committee; Dr. Paul J Schilling and Dr. Kazim M Akyzlu for their encouragement, insightful comments, and hard questions. I am also grateful to Dr. Paul D Herrington and Dr. David Hui for their valuable advice and guidance at different stages of my study.

I thank my fellow lab mates Amer Hussain, Anvesh Nallablli, Mosleh Uddin, Pratik Sarker, and Jose Enrique Rubio in the Department of Mechanical Engineering, University of New Orleans (UNO); for the stimulating discussions, help in the software works, and for all the pleasant time we have had in the last two years. I would like to convey my special gratitude to Monir Hossain and Saiful Arefin Ratul, Department of Electrical Engineering, UNO; for helping me obtain useful conceptions in the electrical engineering aspects of this work.

Last but not the least, I heartily thank my family; my father Mohammed Habibur Rahman Badal and my mother Aklima Jahan for bringing forth me in this world and supporting me unanimously throughout my life.

Table of Contents

Nomenclature

A	Diode ideality factor
A_c	Overlap area of the capacitor electrodes (m^2)
A_{PV}	Total effective Photovoltaic cell area (m^2)
B	Magnetic field strength (T)
b_e	Effective width of the comb electrodes (m)
b_p	Width of the PZT layer (m)
b_s	Width of the substructure (m)
C_a	Viscous damping of air (Ns/m)
C_p	Piezoelectric capacitance (F)
C_sI_c	Internal (Kelvin-Voigt) damping (Nsm^3)
d	Distance between magnet and coil (m)
d_c	Distance between a fixed and a moving capacitor electrodes (m)
d_e	Electrical damping coefficient (Ns/m)
d_m	Mechanical damping coefficient (Ns/m)
E_c	Young's modulus of the beam (GPa)
E_e	Young's modulus of the comb electrodes (GPa)
E_G	Band energy of semiconductor
E_p	Young's modulus of PZT (GPa)
E_s	Young's modulus of the substructure (GPa)
e_{31}	Piezoelectric constant (C/m^2)
FF	Fill factor
F_e	Electric force at the capacitor electrodes (N)

F_r	Magnitude of point load at the tip (N)
h_c	Height of the coil (m)
h_m	Height of the magnet (m)
h_p	Height of each PZT layer (m)
h_s	Height of the substructure (m)
I_c	Area moment of inertia of the beam (m^4)
I_{PH}	Photo current (A)
I_S	Cell saturation of dark current (A)
I_{SC}	Short circuit current (A)
I_{mp}	Current for maximum power (A)
i_p	Piezoelectric current (A)
k_s	Stiffness of the beam (N/m)
L	Length of the cantilever beam (m)
L_e	Length of the comb electrode (m)
L_i	Self-inductance (H)
L_p	Length of the PZT layer (m)
l	Length of the coil or solenoid (m)
M_t	Tip mass (kg)
m_L	Mass of the cantilever beam (kg)
N	Number of turns in the coil
N_P	Number of parallel cells
N_S	Number of series cells
P_{EM}	Electromagnetic power (μW)

P_{ES}	Electrostatic power (μW)
P_{PE}	Piezoelectric power (μW)
P_{PV}	Photovoltaic power (μW)
Q	Electron charge (C)
R_L	Load resistance (kΩ)
R_S	Series resistance (Ω)
R_{SH}	Shunt resistance (Ω)
r_m	Radius of the magnet (m)
r_c	Radius of the coil (m)
V	Voltage (V)
T_C	Cell's working temperature (℃)
T_{ref}	Cell's reference temperature (℃)
w_b	Base displacement in y direction (m)
w_{rel}	Relative displacement in y direction (m)
Y_0	Magnitude of input excitation (m)
α	Electrical coupling force factor (Tm/Ω)
δ_c	Conversion factor (Tm)
$\delta(x)$	Dirac delta function
ε_{33}^{s}	Permittivity of piezoelectric material in series connection (F/m)
ζ_n	Damping ratio of the beam
η	Conversion efficiency
ϑ	Piezoelectric coupling (Nm/V)
ρ_e	Density of comb electrodes (kg/m^3)

ρ_m	Density of magnet (kg/m^3)
ρ_p	Density of PZT (kg/m^3)
ρ_s	Density of Substructure (kg/m^3)
φ_n	Modal forward coupling (C/m)
χ_n	Modal electromechanical coupling (C/m)
ω	Driving frequency of vibration (Hz or, rad/s)
ω_c	Characteristic cut-off frequency (Hz or, rad/s)
ω_n	Fundamental natural frequency (Hz or, rad/s)

Abbreviations

AM	Air mass
DOF	Degrees of freedom
EH	Energy harvesting
EM	Electromagnetic
ES	Electrostatic
FEA	Finite element analysis
FEM	Finite element method
MEMS	Microelectromechanical systems
MPPT	Maximum power point tracking
MsM	Magnetostrictive materials
NA	Neutral axis
OSC	Organic solar cell

PE	Piezoelectric
PV	Photovoltaic
PVDF	Polyvinylidene fluoride
PZT	Lead zirconate titanate
RF	Radio frequency
RMS	Root mean square
SHM	Structural health monitoring
S-N	Stress-Life (number of cycles)
TEG	Thermoelectric generator
WSN	Wireless sensor networks or nodes

List of Figures

List of Tables

ABSTRACT

Hybrid energy harvesting is a concept applied for improving the performance of the conventional stand-alone energy harvesters. The thesis presents the analytical formulations and characterization of a hybrid energy harvester that incorporates photovoltaic, piezoelectric, electromagnetic, and electrostatic mechanisms. The initial voltage required for electrostatic mechanism is obtained by the photovoltaic technique. Other mechanisms are embedded into a bimorph piezoelectric cantilever beam having a tip magnet and two sets of comb electrodes on two sides of its substructure. All the segments are interconnected by an electric circuit to generate combined output when subjected to vibration and solar illumination. Results for power output have been obtained at resonance frequency using an optimum load resistance. As the power transduced by each of the mechanisms is combined, more power is generated than those obtained by stand-alone mechanisms. The synergistic feature of this research is further promoted by adding fatigue analysis using finite element method.

Keywords: hybrid energy harvester, photovoltaics, piezoelectricity, electromagnetism, electrostatic mechanism, fatigue

1. Introduction

1. 1 Fundamentals of Energy Harvesting

Energy harvesting (EH), also known as power harvesting, refers to the process of extracting energy from ambient sources and storing it in a consumable electrical energy form [1]. Energy scavenging and power scavenging are the terms that are also used to describe the process. In general, an energy harvester consists of three main components: the generator (EH device) that converts ambient energy into electrical energy, the conditioning circuit (e.g., voltage booster and rectifier) that amplifies and regulates the generated voltage, and the storage element which can be a battery or a super-capacitor. Figure 1 illustrates how a simple energy harvesting scheme is employed to convert and store ambient energy into electrical energy [2]. Both the stored energy or the converted energy without storing can be used by low-power portable devices and various sensor nodes for applications of sensing, actuating, and sending wireless signals.

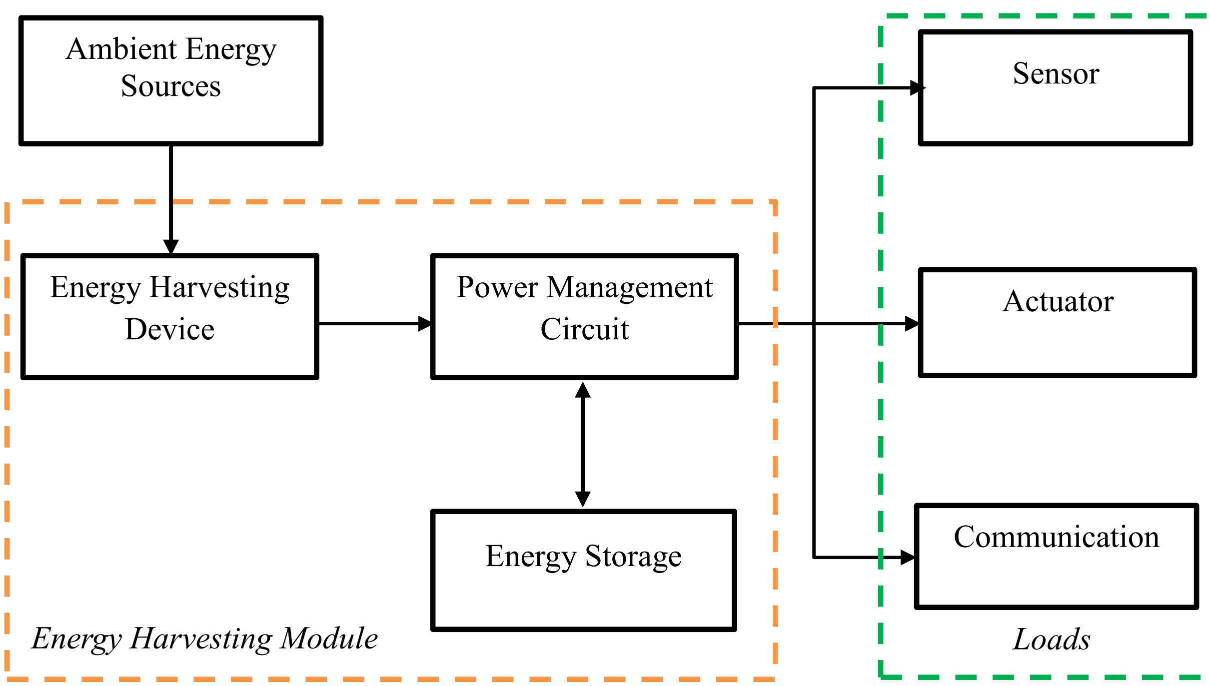

Figure 1.1: Simple Illustration of the energy harvesting process

1.1.1 State of the Art

Energy harvesting technology facilitates the creation of autonomous, self-powered electronic systems that do not rely on battery for operation. There has been a surge of research in the area of energy harvesting in the last few decades [1−46]. This increase in research has been invigorated by the modern advances in wireless technology such as wireless sensor networks (WSNs) and low-power electronics such as the microelectromechanical systems (MEMS). Vigorous implementations of such devices can be observed in the fields of self-powered sensors and actuators, structural health monitoring (SHM), surveillance, aerospace, automobiles, biomedical science, tracking animal migration, and plenty of new dynamic and prospective applications. In most cases, the conventional battery is used as the power supply for the advanced portable electronics and wireless sensors; which creates problems such as finite lifespan, weight limitation, and need for maintenance. Again, the disposal of these batteries can be hazardous for the environment too. Consequently, to achieve the full potential of the MEMS and WSNs, it is essential to develop practical solutions for the self-powering of these devices. The harvested energy from the ambient environment can be a vital means to replace or recharge the batteries and thus can ensure a prolonged lifespan of the power supply [3, 5, 6].

Reliable power supply is becoming a critical issue in the applications of WSNs. External chemical battery is not an appropriate solution because of the factors mentioned above. Ultimate long-lasting solution should be independent of the limited energy available; a self-renewable energy source from the environment that can continually replenish the energy consumed in the wireless sensors. Thus, the ambient energy that is typically lost or dissipated in the environment is exquisitely recovered and used to power the wireless sensors and MEMS devices, significantly extending their operational lifetime.

With a view to harvesting energy from the ambient sources, a variety of techniques are available; including photovoltaics, rotor-dynamics, thermoelectricity, piezoelectricity, and so on. Since, solar energy is the most prolific one among all the sources; it is a customary choice to apply photovoltaic technique for energy harvesting [12−16]. RF energy can also be utilized to power up micro-sensors wirelessly [17]. As for thermal energy, voltage potential difference is built up due to thermal gradient formed between two conductors [18, 19] to serve the same purpose. But, mechanical vibration has gained much popularity as a source as it combines energy harvesting with vibration reduction purpose; generating electrical energy in the process of vibration isolation [1−11, 20−52]. However, an energy harvester adopting a single method can hardly provide sufficient energy even for the microelectronic devices. One possible solution could be a hybrid energy harvester that combines several transduction methods to amplify the output. Such device has the ability to harvest energy from several sources to provide robustness against variable environmental conditions, effectively allowing the system to operate in the case when energy is no longer available from one or more of the ambient sources [8, 41−52].

1.1.2 Applications and Benefits of the Harvested Energy

Now-a-days, the interest in harvesting energy from the environment is increasing rapidly. Harvested energy from the ambient sources (usually at micro level) can be used to –

(a) power MEMS and WSNs,

(b) replace batteries in MEMS and WSNs

(c) recharge batteries and capacitors, and

(d) increase lifespan of the power supply.

Thus, the applications of energy harvesting technology can be seen widely in the fields of self-powered WSNs and MEMS devices which are used in:

- **Environmental Monitoring**
  - Habitat Monitoring (e.g., temperature and humidity)
  - Integrated Biology
- **Structural Monitoring**
  - Damage detection and health monitoring of bridges, high-rise or sophisticated structures
- **Interactive and Control**
  - Radio frequency identification device (RFID), Real Time Locator and Tags
  - Building and Automation
  - Transport Tracking and vehicle sensors
  - Oil refinery monitoring
- **Surveillance**
  - Pursuer-Evader
  - Intrusion Detection
  - Interactive museum exhibits
  - Unmanned Aerial Vehicles
- **Medical remote sensing**
  - Emergency medical response
  - Monitoring, pacemakers, and defibrillators
  - Self-powering the medical implants
- **Military applications**
- **Automotive and Aerospace structures**
- **Micro-robotics and smart electronics**

It is a fact that about 90% of the WSNs depend on the harvested energy for power requirement [1]. The substantial benefits provided by the energy harvesting technology are listed below:

(a) Overcoming from the limitations of non-regenerative sources such as batteries
(b) Long lasting power supply
(c) No chemical disposal
(d) Cost effectiveness
(e) Safety and reliability
(f) Maintenance free
(g) No charging points
(h) Operable to inaccessible sites
(i) Flexibility
(j) Only possible means to some applications

1.2 Sources of Energy

The available and potential sources of ambient energy can be broadly classified into non-regenerative and regenerative sources. The non-regenerative sources include batteries, fuel cells, micro-combustors, turbine, and heat engines while the regenerative sources are solar, wind, temperature and salinity gradient, radio frequency, and kinetic energy such as vibration, human locomotion and so on. Scope of some of the regenerative sources are discussed below:

1.2.1 Ambient Illumination

Ambient illumination refers to the outdoor and indoor solar radiation. Solar power systems are one of the most commonly considered strategies of energy harvesting [12]. These systems consist of the array of solar cells and signal processing circuitry. Power from solar cells

results from the photovoltaic effect, which is the direct conversion of incident light into electricity [13, 14]. Photons, generated from sunlight are absorbed (producing proton holes), stimulating current orthogonal to the flow of proton holes. The advantages of solar array systems include their ease of integration, modularity, lack of emission or noise, lack of moving parts and use of a readily available resource, i.e. sunlight. Disadvantages of solar systems include the additional signal processing circuitry required to provide high quality continuous current at a specific voltage; variability in quality and amount of power generation and requirement of relatively large surface area. Other disadvantages of PV systems that are prohibitive to MEMS applications are low conversion efficiencies, high cost, and the spotty availability of sunlight.

In direct sunlight at midday, the power density of solar radiation on the earth's surface is roughly 100 mW/cm^3. Silicon solar cells are a mature technology with efficiencies of single crystal silicon cells ranging from 12% to 25%. Thin film polycrystalline, amorphous silicon solar cells, and organic solar cells (OSC) [16] are also commercially available and cheaper than the single crystal silicon, but have lower efficiency. As seen in the Table 1, the power available falls off by a factor of about 100 on overcast days. However, if the target application is outdoors and needs to operate primarily during the daytime, solar cells offer an excellent and technologically mature solution. Available solar power indoors, however, is drastically lower than that available outdoors (Table 1).

1.2.2 Mechanical Vibration

Among the renewable energy sources, mechanical vibration is deemed to be one of the most attractive for its power density, versatility, and abundance [17, 18]. It can deliver reasonably high-power density and allows versatile transduction possibilities to be adopted by the energy harvesters including piezoelectric, electromagnetic, electrostatic, and magnetostrictive

methods. In general, frequency and acceleration are the key parameters to assess vibration sources. The higher those values, the larger provided power to the energy harvesters.

Vibrations exist in industry, buildings, home appliances, automotive, and so on where the amplitudes of acceleration prevail below 9.81 m/s^2 and frequencies range from 10 Hz to 1000 Hz [4]. Most of the civil vibration sources such as truck engine, microwave oven, and kitchen blender have low frequency vibration up to 150 Hz and their accelerations are usually less than 0.5 g (1g = 9.8 m/s^2). For long-span bridge, frequency and acceleration become even lower as < 0.1 Hz and 0.0001 ~ 0.1 g, respectively. On the contrary, there are significant ambient vibrations available on the aerospace structures: up to 1g between 300 Hz ~ 1 kHz.

1.2.3 Thermal Energy

Thermal gradients in the environment are directly converted to electrical energy through the Seebek effect with thermoelectric generators (TEGs) [18, 19]. Temperature differential between opposite segments of a conducting material results in heat flow and consequently charge flow. To carry the dominant charge carriers of each material as a result of heat flow from the high temperature side to the low temperature side, thermoplies (laminated sheathings) are constructed consisting of *n*- and *p*-type materials electrically connected at the high temperature junction and thus, establishing in the process a voltage difference across the base electrodes. The generated voltage and power is proportional to the temperature differential and the Seebeck coefficient of the thermoelectric materials. It is necessary to create large thermal gradients to obtain practical level of voltage and power. In micro-systems, temperature differences greater than 10°C are quite rare and consequently, low amount of voltage and power are produced.

The substantial advantages of the TEGs compared to the vibration-based energy harvesters are that they do not have any moving part and can operate for long time with little

noise and emissions. Yet, the commercial applications of the TEGs have not been flourished due to the material constraints such as the toxic content, low melting point, low conversion efficiency of the intermetallic compounds used in the thermocouple modules. Again, the energy conversion is relatively inefficient during low thermal gradients. The disadvantages continue as the dimensions and weight of the devices are too large to integrate them with MEMS and WSN technologies [19].

1.2.4 Human Power

Human power, in both active and passive form, has attracted much interest owing to the availability of human motions and body heat. Previous studies have shown that several dozens of Watts are exhausted in the human gait [20] which can be a feasible source for the human energy harvesters. Flexible devices that can be worn or attached to the human body to harvest the strain energy from human movements at low frequency have been vigorously studied in recent years [20–24]. In most cases, the stand alone energy conversion technique using materials like PZT nanowires [21], PZT ribbons [22], polyvinylidene fluoride (PVDF) nanofibers [23], and zinc oxide (ZnO) nanowires [24] have been applied onto flexible substrates in order to harvest energy from low frequency human motions. It has been shown that energy harvesting for body-worn or body-attached applications can potentially provide the solution for the power requirement of the modern low-power devices with the increase in mobility and independence of the user.

1.2.5 Comparison of the Energy Sources

So far, a brief overview of some of the key regenerative sources of ambient energy has been presented. The other mentionable regenerative sources are acoustic noise, RF, salinity gradients, wind energy which are not as attractive as the above mentioned ones. However, it is important to know the power densities of the non-regenerative sources before recommending the

replacements for them. A comparison of the power densities of some of the energy sources is shown in Table 1.1.

Table 1.1 Comparison of power densities of various sources [4,11]

Source	Power Density [$\mu W/cm^3$] 1 year life time	Power Density [$\mu W/cm^3$] 10 years life time
Solar (outdoors)	15,000 (sunny)[a], 150 (cloudy)[a]	15,000 (sunny)[a], 150 (cloudy)[a]
Solar (indoors)	6 (office desk)	6 (office desk)
Vibrations	375	375
Temperature gradients	15 at 10^0C gradient	15 at10^0C gradient
Acoustic Noise	0.003 at 75 Db, 0.96 at 100 Db	0.003 at 75 Db, 0.96 at 100 Db
Human Power	330	330
Batteries (non-rechargeable Li)	45	3.5
Batteries (rechargeable Li)	7	0
Fuel Cell (methanol)	280	28

[a] measured in $\mu W/cm^2$

Based on these data, it is evident that solar energy and vibrations offer the most attractive energy harvesting possibilities as both of them meet the power density requirement in environments that are of interest for MEMS and WSN.

1.3 Hybrid Technique of Energy Harvesting

Typically, a hybrid energy harvester is one that employs more than one energy harvesting technologies simultaneously in order to obtain more power than a stand-alone energy harvester. Actually, the concept of a hybrid energy harvesting can be illustrated into two points of view:

(1) harvesting from single source (e.g., vibration) and

(2) harvesting from several sources (e.g., vibration, solar, and thermal).

The hybrid energy harvester has received great attention for its important advantages, such as being clean, stable, having high energy density, and a wide frequency band. The ability to harvest from several sources provides robustness against varying environmental conditions and effectively allows the system to remain online in the case where ambient energy is no longer available from one or more of the sources. Consequently, it becomes important and at the same time challenging to select appropriate energy sources and consider a robust multifunctional design for the hybrid energy harvester.

1.4 Literature Review

Harvesting the waste energy from the ambient sources for powering the low-power electronic components has gained great attention in the last two decades. A number of review articles have been published [1, 3−7] proving the necessity of energy harvesters in manifold applications. Solar, thermal, wind, RF, and kinetic energy can be converted to usable electrical energy either by the stand-alone or hybrid mechanisms to autonomously power the WSNs and MEMS devices [1−11]. Significant number of investigations have been reported by the researchers on the standalone energy harvesters based on photovoltaic [12−17], thermoelectric [19, 20], piezoelectric [25−29], electromagnetic [30−33], electrostatic [34−37], and magnetostrictive [38−40] methods.

To improve the energy conversion efficiency and increase power density of energy harvester, the development of hybrid energy harvester based on multi-transduction mechanisms has become significantly important. However, the most effective hybrid generators are often those that harvest energy from the same source, such as vibration-based hybrid piezo-electromagnetic generators [41, 42]. The simplest one of such generators consists of a piezoelectric cantilever beam with a magnet as the proof mass and electromagnetic coils

surrounding the magnet. As the beam oscillates, stresses are induced in the piezoelectric beam, producing electricity, and the magnet moves away from and toward the coil, inducing a current through the wire. A good variety of this device has been published in recent years [31, 41−45].

The hybrid energy harvester has received great concern because of its important advantages, such high energy density, stability, multi-functionality, and a wide frequency band. For instance, a general spring-mass-damper model was presented by Williams and Yates [31], where the harvested electrical energy was equivalent to the energy dissipated in the electrical damping. The spring-mass-damper model was widely used by simplifying the effect of two complex mechanisms into viscous damping. Shan *et al*. [41] presented an energy harvester using a piezoelectric and suspension electromagnetic mechanism to enlarge the frequency bandwidth and obtain a larger energy output. But the design of the energy harvester was based on meso-scale architecture having a large volume which limits the application fields. Larkin and Tadesse [42] presented a multimodal energy harvesting device that was able to generate a maximum RMS power output of 120 mW from the electromagnetic system at 5 Hz and 0.8 g acceleration; and 4.23 mW from the piezoelectric system at 20.2 Hz and 0.4 g excitation acceleration. Khalig *et al.* [43] and Yang *et al.* [44] investigated the hybrid energy harvesters integrated with piezoelectric and electromagnetic energy harvesting mechanisms. However, the maximum output voltage is only 0.84 V, which is difficult to be used for supplying power for the subsequent load. Challa *et al*. [45] were able to generate an output of 332 μW at 21.6 Hz from a cantilever beam hybrid energy harvester. The harvester produced a 30% increase in power output compared to 257 μW and 244 μW generated from the stand-alone piezoelectric and electromagnetic energy harvesting devices, respectively.

Hybrid energy harvesters combining piezoelectric and electrostatic methods have also shown promising outcomes [46−48]. Designs and Characterizations of such hybrid devices were presented by Khbeis *et al.* [46-47] where simultaneous transductions of piezoelectric and electrostatic technique were investigated. Eun *et al.* [48] developed a flexible hybrid strain energy harvester using piezoelectric and electrostatic conversion.

Goudarzi *et al.* [50] presented a hybrid harvesting technique by simultaneous use of the piezoelectric and pyroelectric effect, where it was proved that harvesting energy by the hybrid technique produced almost 38 % more power than the stand-alone piezoelectric effect with PZT materials. To take advantage from both light and vibration energy sources, a hybrid indoor ambient light and vibration energy harvesting scheme was proposed by Yu *et al.* [27] where a small-scale amorphous-silicon (a-Si) solar panel was presented that could work in low light illumination. The output voltage was increased by using the PZT MEMS piezoelectric cantilever arrays architecture. With some advanced power conditioning techniques, the experiment results showed that the hybrid energy harvester achieved a maximum efficiency of 76.7%. Colomer-Farrarons *et al.* [40] proposed and demonstrated a hybrid system that harvested energy from indoor light (solar), vibration (piezoelectric), thermoelectric, and electromagnetic to deliver approximately 6.4mW power output.

1.5 Research Objective

The primary objective of the literature is to model and analyze a linear hybrid generator that can harvest energy from both vibration and ambient illumination (mainly sunlight) without any power supply from non-regenerative sources like batteries or fuel cells. This device offers increased power output and thus, good efficiency as it combines the output obtained from

photovoltaic (PV), piezoelectric (PE), electromagnetic (EM), and electrostatic (ES) mechanisms simultaneously.

With a view to meet the objective, an overview on the energy harvesting technology is presented with necessary illustrations about the available ambient sources and the possible transduction mechanisms to harvest energy from them. Besides, characterization of the hybrid technique is also exhibited in light of literature survey to facilitate the conception of hybrid energy harvester. The physical configuration and the mathematical model are presented with necessary illustrations.

The modeling of the hybrid energy harvester is done in ANSYS Workbench 2015 where the modal and structural analysis are conducted using finite element method (FEM). As the hybrid model is subjected to transverse vibration, it takes into account the necessity of the fatigue analysis to verify the reliability of the structure. Therefore, the fatigue criteria have also been determined by conducting the finite element analysis (FEA) and studying the standard Stress-Life Curves (S-N Curves) for the materials used to design the hybrid energy harvester model.

2. A Theoretical Context on the Hybrid Energy Harvesting

2.1 Useful Techniques for Hybrid Energy Harvesters

One of the most effective ways to enhance the power density of energy harvesting devices is to use multiple transduction methods on one device. A hybrid energy harvesting device combines more than one of the energy harvesting technologies to create a more efficient unit. Depending on the sources available and type of transducers used, the device will either have multiple generators driven by the same energy source or will harvest from more than one energy source at the same time. Some useful techniques of transduction are discussed in this section which are in practice to harvest energy from the ambient sources.

2.1.1 Vibration-based Techniques

Vibration energy harvesting has emerged as one of the amazing alternatives to battery for supplying power to MEMS and WSNs [1–10]. As vibrations are present almost everywhere, even in remote locations of constructions, they are a preferable energy source for this purpose. Vibrations exist in industry, buildings, home appliances, automotive systems, and so on where the amplitudes of acceleration prevail below 9.81 m/s^2 and frequencies range from 10 Hz to 1000 Hz [3, 4]. It can deliver reasonably high-power density and allows versatile transduction possibilities such as, piezoelectric, electromagnetic, electrostatic, and magnetostrictive methods [3−7]. The working principle of some of these transduction methods are described below.

2.1.1.1 Piezoelectric System

In piezoelectric generators, the displacement produces mechanical stress in the piezoelectric material, which affects the physical position of the inherent electrical dipoles, thus induces an output electrical voltage [1]. The basic piezoelectric transducer features a unimorph

or a bimorph cantilever beam with an additional seismic mass adhered to the tip to increase the effective mass. Unimorphs consist of a single piezoelectric layer while a bimorph consists of two piezoelectric layers bonded together to form either a *series* or a *parallel*-type configuration. Vibration forces cause a mechanical oscillation of the tip and produce an alternating stress pattern in the piezoelectric material. If the seismic mass load is applied in transverse direction, i.e., the same direction of the oscillation, then it is known as the 33-mode. The other variety is the 31-mode where the load is applied in the longitudinal direction, i.e., perpendicular to the oscillation. These are illustrated in Figure 2.1 where F is the applied load.

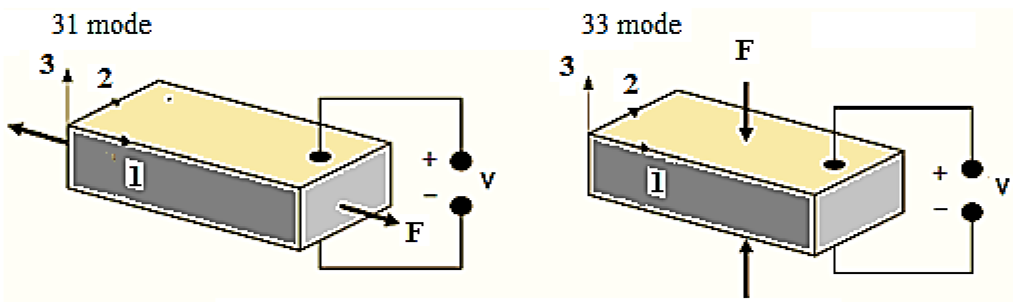

(a) (b)

Figure 2.1: Loading for piezoelectric structures: (a) 31-mode and (b) 33-mode

An electric AC voltage is generated at the electrodes of the piezoceramic via the direct piezoelectric effect. This voltage is in phase with the mechanical oscillation as the mechanical stress varies with the stroke amplitude. The piezoceramic layers of the bimorph configuration shown in Figure 2.2 (a) are connected in *series*. Each piezoceramic layer can be represented as a current source in parallel with its internal capacitance. Figure 2.2 (b) displays the *series* connection of the identical piezoceramic layers of the bimorph configuration shown in Figure 2.2(a).

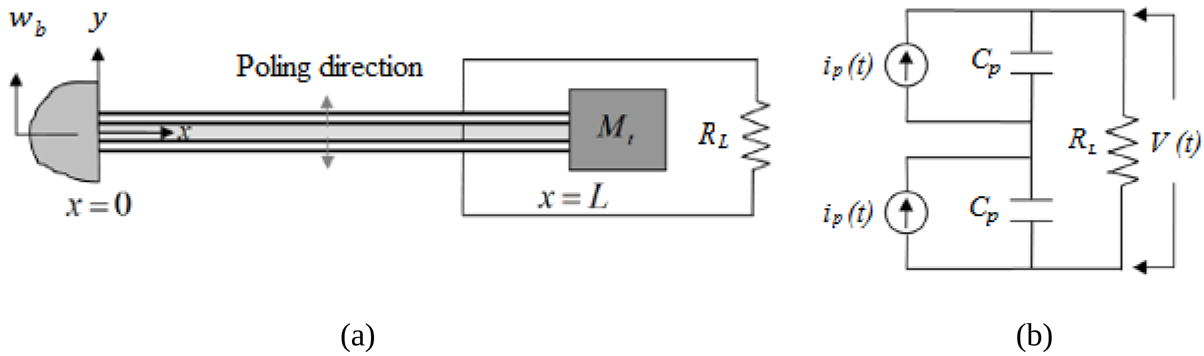

Figure 2.2: Electrical circuit representing the series connection of the piezoceramic layers

PE mechanism is the most widely used vibration-based technique due to its ease of fabrication and application, and high voltage output without bias input [1, 2]. Therefore, it has been applied in the proposed hybrid model as an important contributor in power generation.

2.1.1.2 Electromagnetic System

Electromagnetic power conversion results from the relative motion of an electrical conductor in a magnetic field. Typically, the conductor is wound in a coil to make an inductor. The relative motion between the coil and magnetic field causes a current to flow in the coil. This is similar to the general model described and voltage produced is given by Faradays law:

$$V = NBl\frac{dy}{dt} \tag{1}$$

where N is the number of turns in the coil, B is the strength of the magnetic field, l is the length of one coil ($2\pi r_c$), and y is the distance the coil moves through the magnetic field.

One of the most effective ways of producing electromagnetic induction for energy harvesting is with the help of permanent magnets, a coil and a resonating cantilever beam [8]. Since the late 1990s, various researchers [31-33] have identified the techniques employed to

generate power from electromagnetic resources. The electromagnetic generators designed have the advantage of being enclosed and can be protected from the outside environment.

Electromagnetic induction provides the advantage of improved reliability and reduced mechanical damping as there would not be any mechanical contact between any parts. Like the PE method, EM mechanism does not require any bias voltage [26]. However, materials for electromagnetic transduction are bulky in size and are complicated to integrate with MEMS [27]. Moreover, it is convenient for large deflections [33] which imposes some additional limitations during applications.

2.1.1.3 Electrostatic System

In contrast, ES method requires a DC bias voltage to charge the capacitor plates or electrodes which are oscillated in a dielectric medium to generate cyclic variation in capacitance and thus converts mechanical energy into electrical energy [2, 4]. Another method can be an electret-based (stable electrically charged dielectric material) transduction that polarizes the capacitance when subjected to vibration and does not require the charging and discharging cycles. A state of the art electrostatic MEMS power generator was presented by Tao *et al.* [6] that operates at 125 Hz harvesting an overall power of 0.12 μW at an acceleration of 0.2 g.

The most general electrostatic harvesters can be classified into three varieties of configuration based on the motion of the proof mass relative to the substrate [4]:

(a) In plane gap closing,

(b) In-plane overlap varying, and

(c) Out-of-plane gap closing

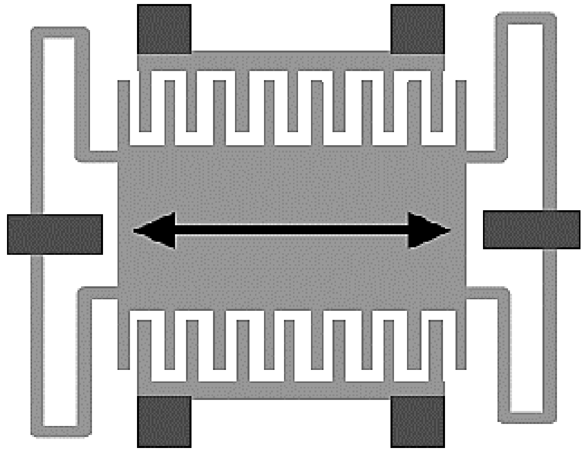

(a) Top view (x-z plane)

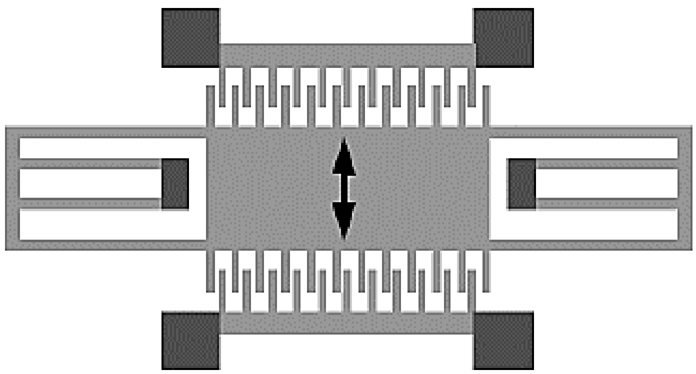

(b) Top view (x-z plane)

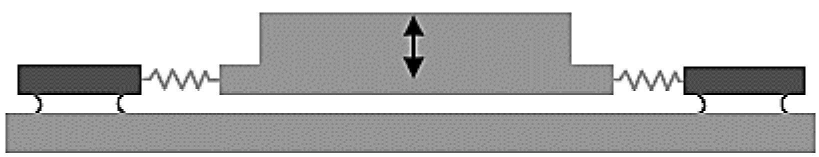

(c) Side view (y-z plane)

Figure 2.3: Three different topologies of vibration based electrostatic converters – (a) In plane gap closing, (b) In plane overlap varying, and (c) Out of plane gap closing; where the arrows show the direction of motion [4]

Figure 2.3 shows the three basic comb drive electrostatic configurations that have already been implemented in operational microsystems such as inertial sensor, accelerometers, resonator, and positioning devices. Among these topologies, out of plane configuration has been selected for the proposed design because of the vertical displacement in *y* direction of the cantilever

beam. Further illustration has been shown in Figure 2.4 where the three motions of comb electrode fingers can be seen evidently [53].

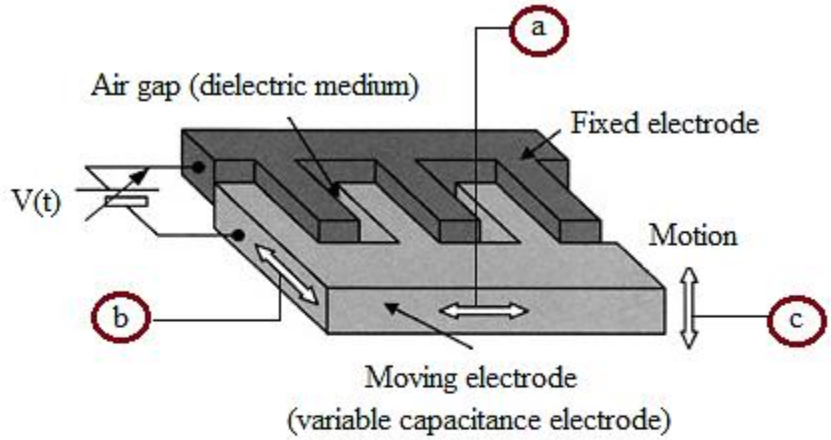

Figure 2.4: Different elementary configurations of an electrostatic comb drive converter where a, b, and c denotes the three different topologies

2.1.2 Photovoltaic Technique

Photovoltaic method, that converts solar energy into electrical energy requires very little maintenance and can provide stand-alone power ranging from microwatts to megawatts. Hence, PV devices can be used to power a variety of energy-consuming systems of multiple scales, ranging from integrated circuits and MEMS to large-scale utility systems [12].

The principles of operation of solar cells are discussed in detail in the literature [13,14]. Photons with energies greater than the energy bandgap of the semiconductor are absorbed, promoting electrons from the valence band to conduction band, leaving a corresponding number of holes in the valence band. If the electron-hole pairs are generated within the depletion region of the p-n junction (or within a minority carrier diffusion length from the edge of each depletion region) the electric field present in the depletion region separates them and drives them through an external load. In addition to traditional Si cells, new materials such as organic semiconductors

as well as high performance inorganic materials are being used for PV with significant progress in efficiency [16].

The tremendous successes of PV on the industrial and utility scales can also potentially be leveraged for the powering of MEMS devices. However, the MEMS applications of PV may require unusual designs and design tradeoffs from the conventional PV point of view. In an energy harvesting MEMS application, area is severely constrained; therefore, a higher efficiency and higher cost multijunction or nonsilicon cell may be appropriate. Other design constraints present in MEMS applications may include flexibility, voltage output, illumination level, and fill factor, potentially leading to significantly different solutions than might be expected from traditional PV module.

2.2 Techniques Applied for the Proposed Model

Since the target is to exploit the two most prolific energy sources, i.e., solar illumination and mechanical vibration, the prime concern has been attributed to the efficient techniques corresponding to these two energy sources. Among the available techniques of transduction, the following four have been selected to model the hybrid energy harvester:

(a) Photovoltaic,

(b) Piezoelectric,

(c) Electromagnetic, and

(d) Electrostatic mechanism

2.2.1 Motivation for Selection

Many literatures have proposed various vibration energy harvesters. However, most of them usually adopt single energy conversion mechanism, such as piezoelectric, electrostatic and electromagnetic transduction. The traditional MEMS vibration energy harvester based on

standalone transduction mechanism can only generate a couple of microwatts power, and also have low output voltage (hundreds of mV). In order to supply power effectively for WSN using vibration energy harvesting technique, the output voltage and power of the energy transducer based on MEMS must be increased. With the addition of photovoltaic method, hybrid generators can be even more productive than the above ones [14].

In order to design a versatile and feasible hybrid energy harvester that can generate power with decent efficiency, the above four mechanisms have been chosen. The bias voltage needed to energize the electrostatic components can be supplied by the photovoltaic module. When subjected to vibration, the proposed hybrid model can generate more power and thus can ensure improved power density of the device.

2.2.2 Comparison of the Transduction Techniques

A brief comparison of the advantages and disadvantages of these mechanisms are illustrated in Table 2.1.

Table 2.1 Advantages and Disadvantages of different energy harvesting mechanisms [13]

Mechanism	Advantages	Disadvantages
Photovoltaic	High energy density No depolarization problem High flexibility Requires less maintenance	Area constrained MPPT circuit requirement Dust and rust sensitive Sensitive to illumination level
Piezoelectric	No external voltage source High voltages of 2-10 V Compact configuration Compatible with MEMS High coupling in single crystals	Depolarization Brittleness in bulk piezo layer Less coupling in piezo PVDF thin film Charge leakage High output impendence
Electromagnetic	No need for smart materials No external voltage source Simple mechanism	Bulky size; magnet and pick up coils Difficult to integrate with MEMS Maximum voltage of 0.1 V
Electrostatic	No need for smart materials Compatible with MEMS Voltages of 2-10 V	External voltage (or charge) required Mechanical constraints needed Capacitive

Based on the above discussion, it is refulgent that each the four mechanisms used to create the hybrid model has distinct characteristics and requires special attention to be configured in a single module. The constraints regarding the design and functional parameters need to be properly addressed in order to obtain desired output and efficiency.

2.3 Established Functional Relationships

While the models for real energy harvesters or converters are somewhat more complicated, the following functional relationships are nevertheless still valid [4]:

- The power output is proportional to the square of the acceleration magnitude of the driving vibrations.
- Power is proportional to the proof mass of the converter, which means that scaling down the size of the converter drastically reduces potential for power conversion.
- For a given amount of input, efficiency of the conversion increases as the power harvested from the sources increases.
- The equivalent electrically induced damping ratio is designable, and the power output is optimized when it is equal to the mechanical damping ratio.
- For a given acceleration input, power output is inversely proportional to frequency. (This assumes that the magnitude of displacement is achievable since as frequency goes down, the displacement of the proof mass will increase.)
- Finally, it is critical that the natural frequency of the conversion device closely matches the fundamental vibration frequency of the driving vibrations.

2.4 Efficiency and Effectiveness

The efficiency of the harvester in terms of the ratio of power can be expressed as follows:

$$\eta = \frac{Total\ Power\ Output}{Total\ Power\ Input} = \frac{P_{out}}{P_{in}} \times 100\%$$

The derivation of the total power output for the proposed model is shown in chapter 4 (Mathematical Model). The input power is comprised of the sum of the solar power input and vibrational base excitation input which can be shown as follows.

$$P_{in} = P_{\ solar} + P_{vib}$$

The effectiveness of the conversion mechanism can be formulated as follows:

$$Effectiveness = \frac{Obtained\ Power\ Output}{Total\ Maximum\ Power\ Output}$$

2.5 Structural Design Aspects of the Hybrid Model

The structural aspects and design considerations of a hybrid energy harvester play the most important role in the performance of the device and consequently, requires a harmonious balance among various design factors. As the piezoelectric ceramics are stiff and crisp, they are not used directly as a stand-alone harvester. A piezoelectric vibrator structure usually composes of a piece of piezoelectric ceramic and a substrate of metal material. Compared to other structural forms of beams, a cantilever beam can obtain the maximum deformation and strain under the same conditions. Besides, the resonant frequencies of a cantilever beam are the lowest [47]. Therefore, the cantilever beam structure is the most popular one for application point of view.

Considering the above facts, the hybrid energy harvester that has been modeled and proposed in this research also consists of a cantilever vibrator with a tip mass. The configuration

is illustrated in chapter 3 with figures and necessary details. But, the theoretical aspects of the structural analysis and effective design are presented here to justify the reasons for developing such a hybrid model and investigating the structural phenomena of it.

2.5.1 Geometric Considerations

The geometry of a piezoelectric cantilever beam and the magnitude and location of tip mass greatly affect the vibration energy harvesting ability. Currently, rectangular cantilever structures are usually adopted for vibration energy harvesting. However, stress concentration phenomenon will appear when piezoelectric cantilevers are bent. In general, stress is the most in the fixed end among all the sections of the cantilever and approaches to zero towards the free end. Therefore, piezoelectric effect of rectangular vibrators cannot be utilized effectively if it is not designed properly. Eventually, this will reduce the efficiency of converting vibration energy to electrical energy. In order to solve this problem, a promising way is to study piezoelectric characteristics of other vibrators with other different geometries [54]. Chen *et. al* [55] compared three different structures of piezoelectric vibrator – rectangular, trapezoidal, and triangular cantilever beams under the same operating conditions. It was demonstrated that the distribution of strain can be improved effectively in the triangular structure, which will be useful to harvest more vibration energy in practice.

2.5.2 Modal Analysis

Modal analysis is the study of the dynamic properties of structures under the excitation of vibration. The frequencies at which vibration naturally occurs, and the modal shapes which the vibrating system assumes are properties of the system, and can be determined analytically using Modal Analysis. The majority of structures can be made to resonate, i.e. to vibrate with excessive oscillatory motion. Resonant vibration is mainly caused by an interaction between the inertial

and elastic properties of the materials within a structure. Resonance is often the cause of, or at least a contributing factor to many of the vibration and noise related problems that occur in structures and operating machinery. To understand any structural vibration problem clearly, the resonant frequencies of a structure need to be identified and quantified. Today, modal analysis has become a widespread means of finding the modes of vibration of a machine or structure. In every development of a new or improved mechanical product, structural dynamics testing on product prototypes is used to assess its real dynamic behavior

Modes are inherent properties of a structure, and are determined by the material properties (mass, damping, and stiffness) and boundary conditions of the structure. Each mode is defined by a natural (modal or resonant) frequency, modal damping, and a mode shape (i.e. the so-called “modal parameters”). If either the material properties or the boundary conditions of a structure change, the modes will also change. For instance, if mass is added to a structure, it will vibrate differently. However, the number of degrees of freedom (DOF) in the structure also determines the type of analysis. For finite number of DOF, the modal analysis can be done by using the Lumped Parameter method while the Distributed Parameter method is applied while dealing with infinite number of DOF.

Detailed modal analysis determines the fundamental vibration mode shapes and corresponding frequencies. This can be relatively simple for basic components of a simple system, and extremely complicated when qualifying a complex mechanical device or a complicated structure exposed to periodic wind loading. These systems require accurate determination of natural frequencies and mode shapes using techniques such as finite element analysis (FEA) [39].

The typical vibration energy harvesters operate at the fundamental frequency (the lowest natural frequency in the periodic waveform) that corresponds to the first mode of vibration since it provides the maximum deflection of the structure. The necessity of modal analysis of the vibration energy harvester to identify the fundamental frequency thus becomes prominent and makes it a common practice for the researchers in this field

2.5.3 Stress and Fatigue Analysis

Fatigue is the weakening of a material caused by repeatedly applied loads. When a material is subjected to cyclic loading, it is vulnerable to progressive and localized structural damage which is known as fatigue. In fact, fatigue failures occur due to the application of fluctuating stresses that are much lower than the stress required to cause failure during a single application of stress. It has been estimated that fatigue contributes to approximately 90% of all mechanical service failures. There are three basic factors necessary to cause fatigue:

(1) a sufficiently high value of the maximum tensile stress,

(2) a sufficiently large variation or fluctuation in the applied stress, and

(3) a sufficiently large number of cycles of the applied stress.

The fatigue process usually begins at an internal or surface flaw where the stresses are concentrated, and consists of shear flow along slip planes at initial level. Over a number of cycles, this slip generates intrusions and extrusions that begin to be similar to a crack. A true crack that runs inward from an intrusion region may propagate initially along one of the original slip planes, but ultimately turns to propagate transversely to the plane of the principal normal stress. The modern study of fatigue is generally dated from the work of A. Wohler, a

technologist in the German railroad system in the mid-nineteenth century who was concerned by the failure of axles of railway vehicles due to fully reversed fatigue loading.

2.5.3.1 Stress-Life Diagram (S-N Diagram)

The fatigue criteria of a material can be determined on the basis of the Stress-Life method which is shown schematically by Wohler S-N diagram for two materials in Figure 2.5. The S-N diagram generally plots the nominal stress amplitude S versus the cycles to failure N. There are numerous testing procedures to generate the data required for a proper S-N diagram. Usually, the S-N test data are displayed on a log-log plot with the actual S-N line representing the mean of the data achieved from several tests.

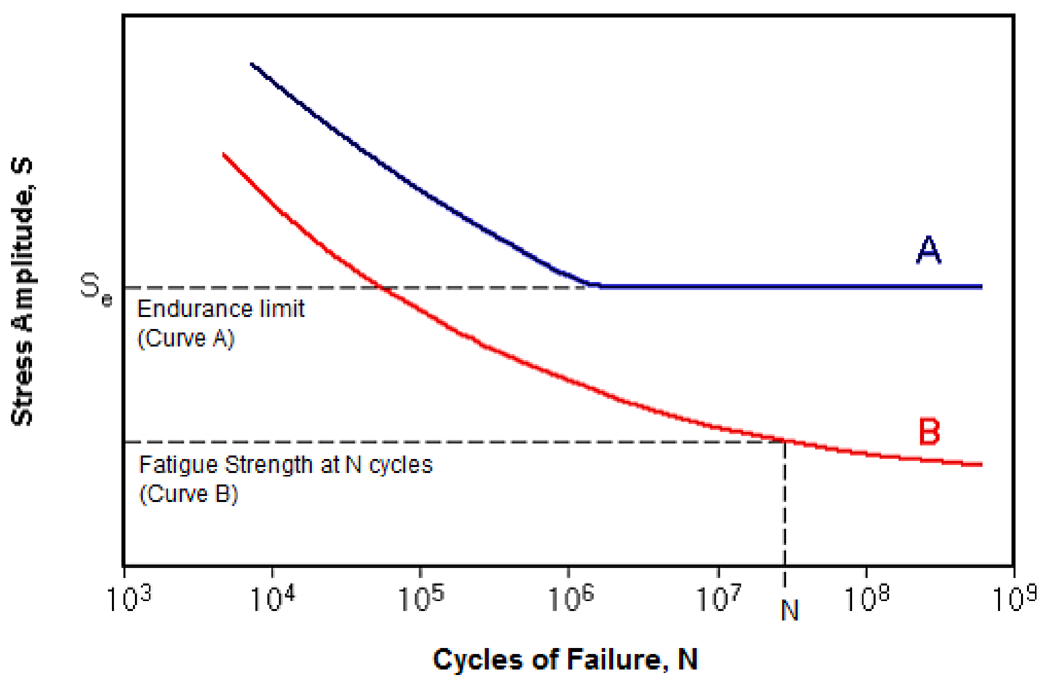

Figure 2.5: Typical S-N Curve for ferrous and non-ferrous materials [57]

2.5.3.2 Fatigue Limit or Endurance Limit

Certain materials have a fatigue limit or endurance limit which represents a stress level below which the material does not fail and can be cycled infinitely. If the applied stress level is

below the endurance limit of the material, the structure is said to have an infinite life. This is characteristic of steel and titanium in benign environmental conditions. A typical S-N curve corresponding to this type of material is shown Curve A in Figure 2.5. Many non-ferrous metals and alloys, such as aluminum, magnesium, and copper alloys, do not exhibit well-defined endurance limits. These materials instead display a continuously decreasing S-N response, similar to Curve B in Figure 2.5. In such cases a fatigue strength (*S*) for a given number of cycles must be specified.

An effective endurance limit for these materials is sometimes defined as the stress that causes failure at $1X10^8$ or $5X10^8$ loading cycles [57]. The concept of an endurance limit is used in infinite-life or safe stress designs. Care must be taken when using an endurance limit in design applications of a structure because the endurance strength can significantly change due to:

- Periodic overloads,
- Corrosive environments, and
- High temperatures.

The number of cycles play an important role to determine the fatigue criteria. High cycle fatigue strength (about 10^4 to 10^8 cycles) can be described by stress-based parameters. A load-controlled servo-hydraulic test rig is commonly used in these tests, with frequencies of around 20–50 Hz. Other sorts of machines such as, resonant magnetic machines can also be used to achieve frequencies up to 250 Hz. Low cycle fatigue (loading that typically causes failure in less than 10^4 cycles) is associated with localized plastic behavior in metals; thus, a strain-based parameter should be used for fatigue life prediction in metals. Testing is conducted with constant strain amplitudes typically at 0.01–5 Hz [57].

The hybrid energy harvester model is subjected to high cycle fatigue stress and Curve B in S-N diagram becomes the determining factor of its fatigue life since it is made of non-ferrous materials. Using FEA in ANSYS Workbench 2015, the maximum bending stress (principal stress) of the hybrid cantilever beam subjected to transverse vibration is determined and the results are presented in chapter 5.

3. Physical Model

3.1 Configuration of the Hybrid Energy Harvester

The proposed hybrid energy harvester consists of a bimorph piezoelectric hybrid cantilever beam with a tip mass at the free end and comb electrodes on two sides of it. The configuration of the hybrid structure and the explanation about the functional aspects are presented in this section.

3.1.1 Hybrid Cantilever Beam Structure

The proposed hybrid energy harvester consists of a bimorph hybrid cantilever beam having an Al substructure (or, shim) with a dimension of 100 mm X 10 mm X 0.75 mm and two layers of PZT (90 mm X 8 mm X 0.40 mm each).

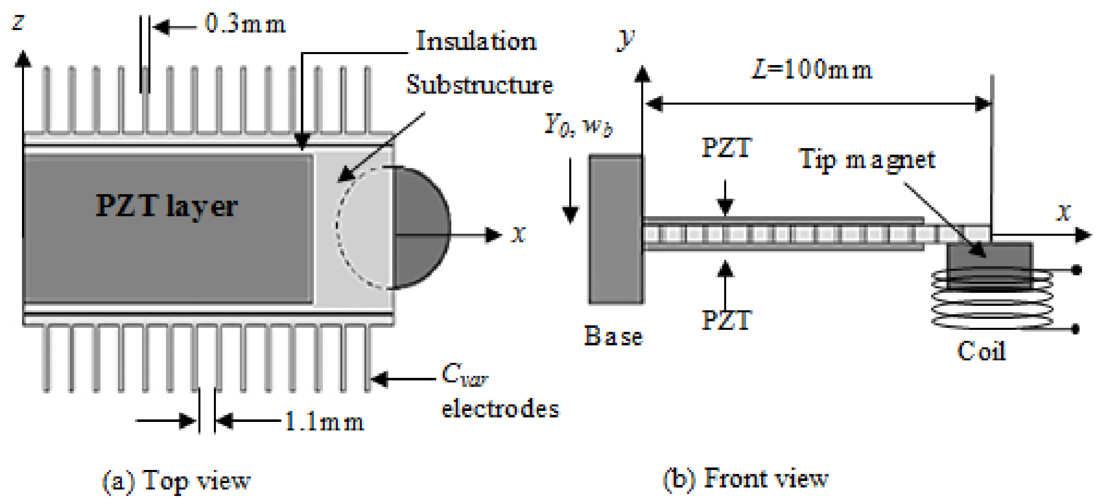

Figure 3.1: Configuration of the bimorph cantilever beam with hybrid structure (figure not drawn to scale)

A simplified 2-D schematic of the hybrid configuration is shown in Figure 3.1 while the actual 3-D configuration is demonstrated in later part of the chapter. Figure 3.1 (a) shows the top

view in x-z plane and the front view in x-y plane is shown in Figure 3.1 (b). Two sets of Cu comb-electrodes (C_{var}) are soldered with the shim by keeping insulations in between. Each set contains 70 electrodes each having the dimension of 9 mm X 0.75 mm X 0.3 mm. The gap between two subsequent electrodes is 1.1 mm. The geometric parameters and physical properties of the hybrid beam are shown in Tables 3.1 and 3.2, respectively.

Table 3.1: Geometric parameters of the hybrid cantilever beam

Geometric Parameter	Value
Length of the cantilever beam, L	0.1 m
Height of each PZT layer, h_p	0.0004 m
Width of PZT, b_p	0.008 m
Effective width of the comb electrodes, b_e	0.0029 m
Width of the substructure, b_s	0.01 m
Height of the substructure, h_s	0.075 m
Area moment of Inertia, I	0.001066 m^4

Table 3.2: Physical properties of the hybrid cantilever beam

Physical Properties	Value
Density of comb electrodes, ρ_e	8960 kg/m^3
Density of PZT, ρ_p	7800 kg/m^3
Density of Substructure, ρ_s	2700 kg/m^3
Density of the Magnet, ρ_m	7400 kg/m^3
Young's modulus of comb electrodes, E_e	117 Gpa
Young's modulus of PZT, E_p	66 GPa
Young's modulus of Substructure, E_s	70 GPa
Young's modulus of the magnet, E_m	160 GPa

Though, the device is a linear one, tuning for achieving the resonance can be done by applying the magnetic technique as discussed in [56]. Besides, the tip mass and length can be optimized to obtain the resonance frequency [62].

3.1.2 Fixed Electrodes or Stationary Capacitors

Complementing the C_{var} electrodes, two similar combs of electrode layers (stationary capacitors) are attached to the base on two sides of the shim keeping 0.4 mm gap with each C_{var} electrode as shown in Figure 3.2. Among the three basic electrostatic configurations – in-plane overlap varying, in-plane gap closing, and out-of-plane gap closing – the last one has been chosen to avoid contacts between the moving and stationary electrodes.

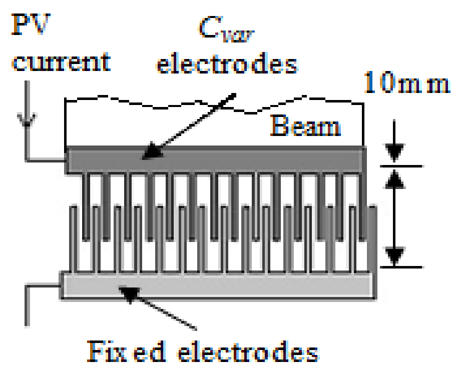

Figure 3.2: Top view of the comb electrodes at one side of the beam

3.1.3 Tip Magnet and Coil

A cylindrical Neodymium Iron Boron (NdFeB) magnet with a radius of 4.2 mm and height of 20 mm is attached at the tip. The density of the magnet material is 7400 kg/m^3 and the Curie temperature is 320°C. The coil or solenoid, surrounding the magnet, is made of Copper and has 600 turns. The radius of the solenoid is 5.2 mm and the height is 25 mm. The gap between the coil and magnet is kept 1 mm. During the movement of the magnet, it has been assumed that there is no contact between the magnet and the coil. The resistance of the coil is 220 Ω and diameter of the wire is 50 micrometers. The magnetic field strength B is considered as 1.18 T.

3.1.4 Photovoltaic Panel

The photovoltaic panel includes four arrays of organic solar cells (OSC) as described by Lewis *et al.* [16] where each array has 20 cells each having an area of 1mm^2. Figure 3.3 depicts the simple configuration of one array of organic cells. The total device area for each array including the gaps is 2.2 cm^2. Therefore, considering four arrays the total device area becomes 8.8 cm^2 where the effective PV area turns out to be 8 cm^2.

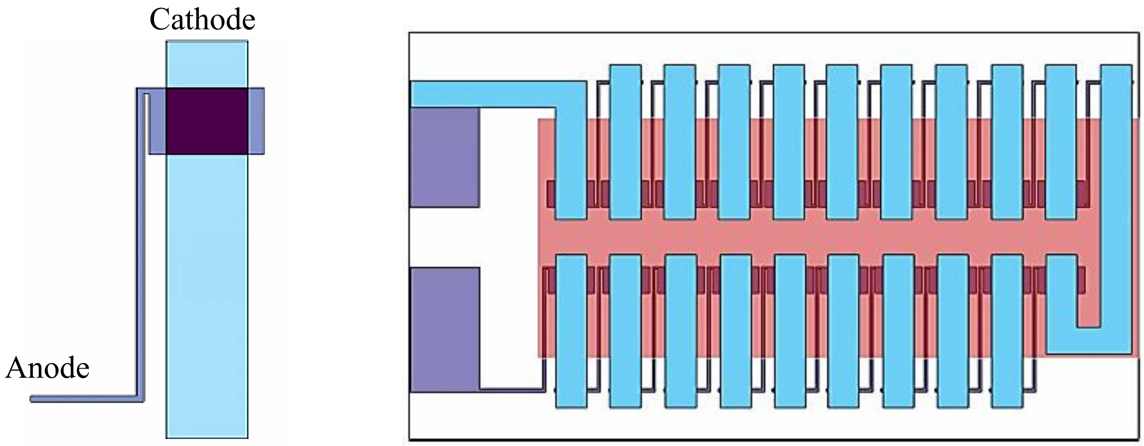

(a) (b)

Figure 3.3: (a) Single organic cell and (b) PV array configuration with 20 cells [16]

3.2 Power Conditioning Circuit

A crucial element for any energy harvesting system is an electrical circuit which can condition and store the ambient energy in an efficient manner. The circuit usually consists of two basic parts- the conditioning part and the storage part. The storage mechanism is out of the scope of the literature as the conversion of energy is the main focus of it. However, the vibration based methods induce AC voltage that has to be converted to DC voltage by rectifiers when combined with the PV generator considering a common load resistance. Therefore, a robust multiple-source

circuit is required to achieve the desired output. A simplified circuit diagram of the proposed hybrid energy harvester is shown in Figure 3.4 where R_L is the common load resistance and the parallel connected PV, ES, PE, and EM generators are represented as G_{PV}, G_{ES}, G_{PE}, and G_{EM}, respectively.

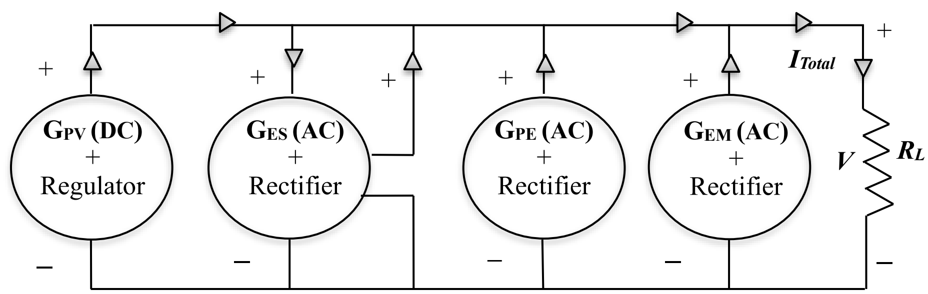

Figure 3.4: System diagram of the proposed hybrid energy harvester exclusive of the storage circuitry

However, in order to obtain enhanced efficiency, the circuit may have a voltage booster, then a rectifier, and finally a multiplier or adaptor before connecting with the load resistance or control cell. These components have not been shown in the above simplified circuit diagram.

3.3 Finite Element Model

Modeling of the hybrid cantilever beam has been done in ANSYS Workbench 2015 with the same dimension as stated above. In this section, the physical domain, boundary and initial conditions, and the mesh generation have been presented.

3.3.1 Physical Domain

The physical domain of the hybrid cantilever beam that has been modeled consists of the bimorph piezoelectric beam with comb electrodes on two sides of the substrate and a cylindrical

tip mass as shown in the Figure 3.5. It has been ensured that all the layers and segments are perfectly bonded. The coil and the complementary fixed electrodes are not considered since the purpose of the finite element analysis is to determine the resonance frequency and the fatigue life of the beam. For the same set of materials, several simulations have been done with different mesh sizes, i.e., a variety of degrees of freedom.

3.3.2 Boundary and Initial Conditions

1. Boundary conditions: The boundary conditions of the hybrid cantilever beam are shown in Table 3.3.

Table 3.3: Boundary conditions for solid domain

	Boundary conditions							
	Displacement (m)			Rotation (degrees)			Moment (Nm)	Shear Force (N)
Name	u	v	w	θ_x	θ_y	θ_z	M	F_r
Free end	-	-	-	-	-	-	0	$m_{eff}\, g$
Fixed end	0	0	0	0	0	0	-	-

2. Initial condition: Initially (at $t = 0$) all DOF are zero except for the vertical displacement $w\ (x, t)$ and the vertical velocity $\dot{w}\ (x, t)$ of the beam which are assumed as follows:

At $t = 0,\ w\ (x, 0) = Y_0$ and $\dot{w}\ (x, 0) = \omega Y_0$

3.5.5 Mesh Generation

The physical domain of the hybrid beam was meshed with the default 3-D quadrilateral-triangular mesh. As the main purpose of the FEA modeling is to do the modal and fatigue

analysis, a finer mesh obviously can help to obtain more precision in the results. But, due to the limitation of element numbers (or degrees of freedom), moderately fine mesh was considered for the analysis. A sample of the generated mesh of the hybrid cantilever beam with tip mass is shown in Figure 3.5.

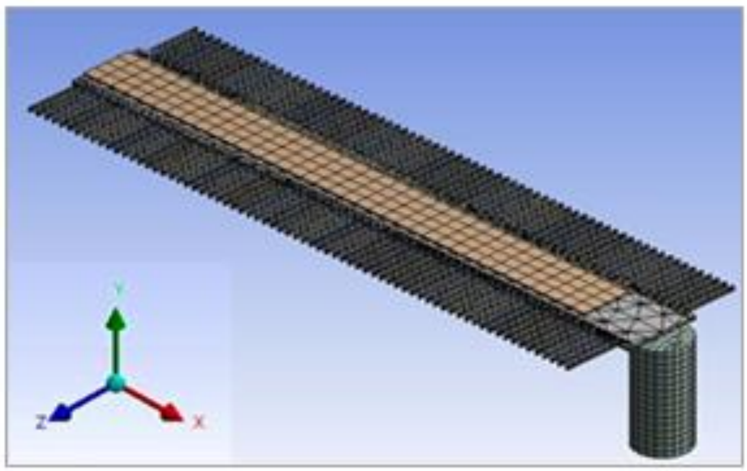

Figure 3.5: Default quadrilateral-triangular mesh of the beam

However, to verify the effective mesh generation, a mesh independence study has been presented in the form of convergence of the fundamental resonance frequency with the increase of degrees of freedom in chapter 5.

4. Mathematical Model

An electromechanical analogy is adopted for the mathematical modeling of the hybrid energy harvester including the basic photovoltaic equations [12, 58] and governing partial differential equation of a cantilever beam in a distributed parameter system under forced vibration [27−29, 60].

4. 1 General Assumptions

The assumptions of the mathematical formulation of the hybrid cantilever beam are mentioned below:

(1) The cantilever beam follows the Euler-Bernoulli beam theory where twisting is not considered.

(2) Shear deformation and rotary inertia are ignored.

(3) Materials of the hybrid structure are linearly elastic.

(4) The piezoceramic and the substructure layers are assumed to be perfectly bonded to each other.

(5) The instantaneous electric fields induced in the piezoceramic layers are assumed to be uniform throughout the length of the beam.

(6) The strain in the PZT layer works in 33 mode as the beam is subjected to transverse vibration.

(7) The C_{var} capacitors attached on two sides of the beam are insulated from the substructure.

(8) The load resistance R_L, the series resistance R_S, and the shunt resistance R_{SH} are constants

4.2 Governing Equations of Power and Associated Expressions

In this section, expressions of power have been presented for each mechanism and finally, the total power output and efficiency formulae have been derived.

4.2.1 Photovoltaic Equations

Considering an array of PV modules as depicted in Figure 4.1, the output current I and output voltage V of a PV array with N_S cells in series and N_P strings in parallel is found from Equation (2) [58].

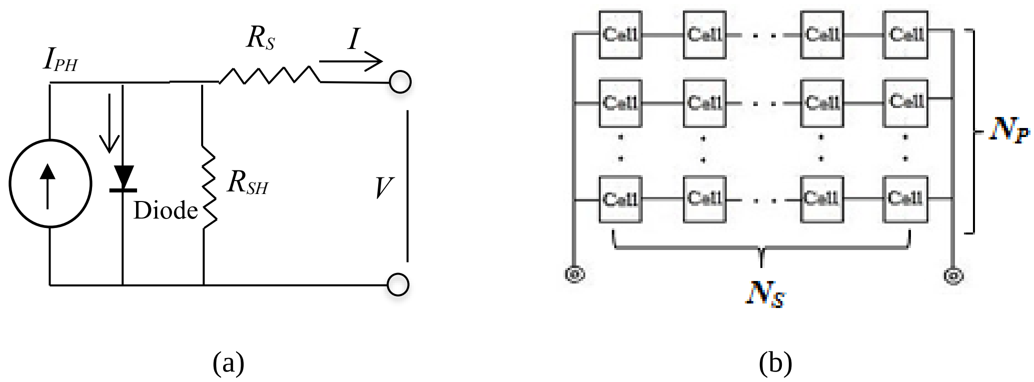

Figure 4.1: (a) Single diode solar cell and (b) PV array configuration

$$I = N_P I_{PH} - N_P I_S \left[\exp\left(\frac{q\left({}^{V}/_{N_S} + IR_S \right)}{{}^{N_P}/_{kT_C A}} \right) - 1 \right] - \frac{\left({}^{N_P V}/_{N_S} + IR_S \right)}{R_{SH}} \qquad (2)$$

where, I_{PH} is the light-generated current or photocurrent, I_S is the cell saturation of dark current, $q = 1.6 \times 10^{-19}$ C is the electron charge, $k = 1.38 \times 10\text{-}23$J/K is Boltzmann's constant, T_c is the cell's working temperature, A is diode's ideality factor (typically between 1 and 2), R_{SH} is the shunt resistance, and R_S is the series resistance. The photocurrent can be calculated as follows:

$$I_{PH} = [I_{SC} + K_1(T_C - T_{ref})]\lambda \tag{3}$$

where, I_{SC} is the short-circuit current of a cell at reference temperature of 25ºC and reference irradiance of 1 kW/m^2, K_1 = 0.032 is the cell's short-circuit current temperature coefficient [58], T_{ref} is the cell's reference temperature, and λ is the solar insolation (irradiance) in W/m^2. The cell's saturation current varies with the cell temperature, which is described as

$$I_S = I_{RS}(\frac{T_C}{T_{ref}})^3 \exp\left[\frac{qE_G\left(\frac{1}{T_{ref}} - \frac{1}{T_C}\right)}{kA}\right] \tag{4}$$

where, I_{RS} is the cell's reverse saturation current at a reference temperature and irradiance, and E_G is the band energy of the semiconductor used in the cell. The reverse saturation current at reference temperature can be approximately obtained as

$$I_{RS} = \frac{I_{SC}}{\left[exp\left(\frac{qV_{OC}}{N_s k T_C A}\right) - 1\right]} \tag{5}$$

However, several parameters determine the performance of a solar cell, namely, the open-circuit voltage, V_{OC} (at I= 0), short-circuit current, I_{SC} (at V= 0), and the so-called fill factor (FF) which is calculated by

$$FF = \frac{I_{mp}V_{mp}}{I_{SC}V_{oc}} = \frac{P_{pv}}{I_{SC}V_{oc}} \tag{6}$$

Where, I_{mp} and V_{mp} are the current and voltage operating points for the maximum power(P_{pv}), respectively. The output power is then calculated by the product of either I and V,

or, I^2 and R_L. However, in terms FF, whose value ranges from 0.5 to 0.82, the maximum photovoltaic power is calculated as follows [16]:

$$P_{pv} = FF \times I_{SC}V_{OC} \tag{7}$$

4.2.2 Piezoelectric Equations

Based on the Euler-Bernoulli assumptions, the coupled governing equation of motion for a bimorph PZT cantilever beam of length L with a tip mass M_t and mass per unit length m_L can be represented as [18] as follows:

$$E_c I_c \frac{\partial^4 w_{rel}(x,t)}{\partial x^4} + C_s I_c \frac{\partial^5 w_{rel}(x,t)}{\partial x^4\, \partial \mathrm{t}} + C_a \frac{\partial w_{rel}(x,t)}{\partial \mathrm{t}} + m_L \frac{\partial^2 w_{rel}(x,t)}{\partial t^2}$$

$$+\vartheta V(t)\left[\frac{d\delta(x)}{dx} - \frac{d\delta(x-L)}{dx}\right] = -[m_L + M_t\delta(x-L)]\frac{\partial^2 w_b(x,t)}{\partial t^2} \tag{8}$$

Here, the sum of the harnonic base displacement $w_b(= Y_0 e^{j\omega t})$ and relative displacement w_{rel} gives the total transverse displacement w at any time t and location x of the beam as follows:

$$w(x,t) = w_b(x,t) + w_{rel}(x,t) \tag{9}$$

The electromechanical coupling term for series connection with the bimorph PZT is given by

$$\vartheta = \frac{e_{31}b}{2h_p}\left[\frac{h_s^2}{4} - (h_p + \frac{h_s}{2})^2\right] \tag{10}$$

Based on the proportional damping (or modal damping), the vibration response relative to the base of the bimorph can be represented as a convergent series of the Eigen functions as mentioned by Erturk *et al.* in his models [27-29].

$$w_{rel}(x,t) = \sum_{n=1}^{\infty} \emptyset_n(x)\, \eta_n(t) \tag{11}$$

where $\emptyset_n$ and η_n are the mass normalized Eigen function and the modal coordinate of the clamped-free beam for the n^{th} mode, respectively. The equation suggests that it requires four boundary conditions in terms of *x* and two initial conditions in terms of *t* for the solution. At the fixed end ($x = 0$),

$$w_{rel} = 0, \qquad \frac{\partial w_{rel}}{\partial x} = 0 \tag{12}$$

At the free end ($x = L$), moment is zero but shear force is equal to the applied force at the tip.

$$M = E_c I_c \frac{\partial^2 w_{rel}}{\partial x^2} = 0 \tag{13(b)}$$

$$F_n = \frac{\partial}{\partial x}\left(E_c I_c \frac{\partial^2 w_{rel}}{\partial x^2}\right) = m_{eff}\, g \tag{13(b)}$$

The modal mechanical response can be obtained from the mass normalized reduced partial differential equation of the governing equation as follows:

$$\ddot{\eta}_n(t) + 2\zeta_n \omega_n \dot{\eta}_n(t) + \omega_n{}^2\, \eta_n(t) + \chi_n V(t) = f_n(t) \tag{14}$$

Here, f_n is the mass normalized tip force on the beam. The backward modal electromechanical coupling term χ_n can be given by

$$\chi_n = \vartheta\, \frac{d\phi_n(x)}{dx} \tag{15}$$

Now, for series connection of PZT, Kirchhoff laws can be applied to the circuit depicted in Figure 3.3 to obtain the capacitance and piezoelectric current.

$$\frac{C_P}{2}\frac{dV(t)}{dt} + \frac{V(t)}{R_L} = i_p(t) \tag{16}$$

where the internal capacitance and the piezoelectric current source terms of the bimorph PZT (for each layer) are,

$$C_P = \frac{\varepsilon_{33}^{s} b_p L_p}{h_p} \tag{17}$$

$$i_p(t) = \sum_{n=1}^{\infty} \varphi_n \frac{d\,\eta_n(t)}{dt} \tag{18}$$

Where the forward modal coupling term φ_n can be given by,

$$\varphi_n = -\frac{e_{31} b(h_p + h_s)}{2}\frac{d\,\emptyset_n(x)}{dx} \tag{19}$$

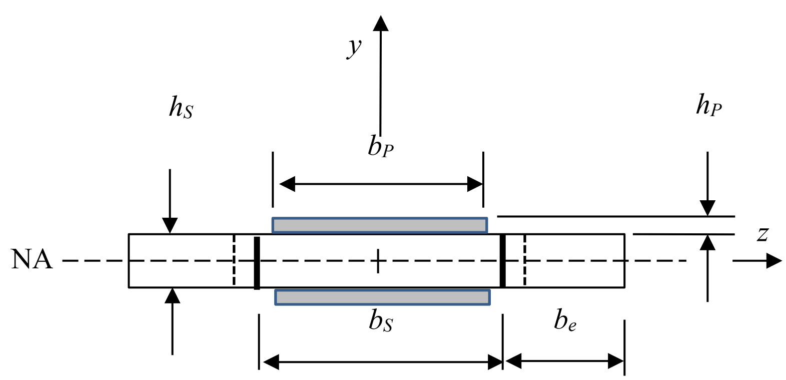

Figure 4.2: Cross-section of the beam considering C_{var}

The cross-section of the hybrid beam in y-z plane is shown in Figure 4.2. The combined bending stiffness E_cI_c and the mass of the beam m can be given by,

$$E_cI_c = \left[\frac{E_s}{24} b_s(h_s)^3 + \frac{E_s}{24}\left\{b_p\left(2h_p + h_s\right)^3 - b_p{h_s}^3\right\} + 2\frac{E_e}{24} b_e h_s^3\right] \times 2 \tag{20}$$

$$m = \rho AL = \rho_s b_s h_s L_s + 2\rho_p b_p h_p L_p + 2\rho_e b_e h_s L_e \tag{21}$$

Therefore, the fundamental natural frequency ω_n of the beam can be determined by,

$$\omega_n = \sqrt{\frac{k_{eff}}{m_{eff}}}$$

$$= \sqrt{\frac{\frac{3E_cI_c}{L^3}}{0.236\, m_L + M_t}}$$

$$= \sqrt{\frac{6\left[\left[\frac{E_s}{24} b_s(h_s)^3 + \frac{E_p}{24}\left\{b_p\left(2h_p + h_s\right)^3 - b_p{h_s}^3\right\} + 2\frac{E_e}{24} b_e h_s^3\right]\right]}{\left[0.236\left(\rho_s b_s h_s L + 2\rho_p b_p h_p L_p + 2\rho_e b_e h_s L\right) + M_t\right]L^3}} \tag{22}$$

where k_{eff} and m_{eff} represent the effective stiffness and effective mass of the beam, respectively. The output power becomes the maximum at the resonance condition, i.e., at $\omega=\omega_n$. The expression of power output $P_{PE}(\omega)$, for the piezoelectric generator at resonance can be given by equation (20) as follows [60]:

$$|P_{PE}(\omega)| = \frac{V^2(t)}{R_L}$$

$$= \frac{R_L(\omega\varphi_n F_r)^2}{[\omega_n^2 - \omega^2(1 + 2\zeta_n\omega_n R_L C_P)]^2 + \left[2\zeta_n\omega_n\omega + \omega R_L[C_P(\omega_n^2 - \omega^2) + \varphi_n\chi_n]\right]^2} \tag{23}$$

4. 2.3 Electromagnetic Equations

The maximum power output expressions for the electromagnetic $P_{EM}(\omega)$ mechanisms at resonance can be given by equations (23) as follows [60]:

$$|P_{EM}(\omega)| = \frac{{Y_0}^2}{2R_L}\left[\frac{m_{eff}\delta_c\omega_c\omega^2}{\sqrt{\left(k_s\omega_c - m_{eff}\omega_c\omega^2 - d\omega^2\right)^2 + \left(k_s\omega - m_{eff}\omega^3 + d\omega_c\omega + \alpha\delta_c\omega_c\omega\right)^2}}\right]^2 \tag{24}$$

where, the electrical coupling force factor, characteristic cut-off frequency, conversion factor, and coil self-inductance are formulized respectively as follows [60, 61]:

$$\alpha = \frac{Bl}{R_L} \tag{25}$$

$$\omega_c = \frac{R_L}{L_e} \tag{26}$$

$$\delta_c = Bl \tag{27}$$

$$L_i = \frac{\mu_0 N^2 \pi {r_c}^2}{h_c} \tag{28}$$

4. 2.4 Electrostatic Equations

The maximum power output expressions for the electrostatic $P_{ES}(\omega)$ mechanisms at resonance can be given by,

$$|P_{ES}(\omega)| = \frac{1}{2}\frac{d_e}{\left(k_s - m_{eff}\omega^2\right)^2 + (d_e + d_m)^2\omega^2}{m_{eff}}^2\omega^6 Y_0^2 \tag{29}$$

where the electrical damping and mechanical damping can be expressed as,

$$d_m = 2\xi_n m_{eff} \omega_n \tag{30}$$

$$d_e = \frac{F_e}{Y_o \omega} \tag{31}$$

where the electric force F_e can be given by,

$$F_e = \frac{\varepsilon_0 A_c V^2}{2d_c^2} \tag{32}$$

where A_c is the overlap area of the comb electrodes and d_c is the gap between two electrodes.

4.2.5 Total Power Output

The total maximum power output P_{total} is the summation of all the outputs minus the electrostatic input $P_{in,ES}$ which is supplied by one of the PV arrays to the C_{var} electrodes to energize the capacitors.

$$\begin{aligned} P_{total} &= P_{out} - P_{in,ES} \\ &= P_{PV} + P_{PE}(\omega) + P_{EM}(\omega) + P_{ES}(\omega) - P_{in,ES} \end{aligned} \tag{33}$$

4.3 Efficiency

As defined in chapter 2, if the input power is a sum of the solar and vibratory power input, then the efficiency η will be,

$$\eta = \frac{P_{out}}{P_{in}} = \frac{P_{out}}{P_{solar} + P_{vib}} \times 100\% \tag{34}$$

The magnitude of vibrational power input P_{vib} is taken as the time averaged vibratory power, i.e.,

$$P_{vib} = \frac{1}{2} m_{eff}\, g Y_0\, \omega_n \tag{35}$$

The solar power input can be given by,

$$P_{solar} = \lambda A_{PV} \tag{36}$$

4.4 Bending Stress

The maximum bending stress (principal stress) in the cantilever beam due to point loading at the tip is given by,

$$\sigma = \frac{Mc}{I_c} \tag{37}$$

where the bending moment M and the maximum perpendicular distance c from the NA can be expressed as,

$$M = P\,L = \frac{3E_c I_c Y_0}{L^3} \times L = \frac{3E_c I_c Y_0}{L^2} \tag{38}$$

$$c = h_p + \frac{h_s}{2} \tag{39}$$

Substituting Equations (38) and (39) into (37), the maximum bending stress can be expressed as,

$$\sigma = \frac{3E_c Y_0 c}{L^2} \tag{40}$$

5. Results and Discussions

5.1. Power and optimum load resistance at the resonance

Using the equations as described in the mathematical model, the results for output power have been obtained in MATLAB R2015a with parameters as shown in Table 5.1. The maximum current (short circuit current) and maximum voltage (open circuit voltage) for an array of organic solar cell have been chosen from the experimental results reported by Lewis et al. [16].

Table 5.1. Nominal simulation parameters (with units as mentioned in nomenclature)

Parameter	Value	Parameter	Value	Parameter	Value
Isc	55 µA [16]	L	0.1	k_s	581.26
V_{OC}	7.8 V [16]	L_p	0.09	δ_c	0.03855
FF	0.5	E_s	70	ω_c	1.2×10^{8}
N_s+N_p	20	E_p	66	α	1.93×10^{-7}
R_L	200 kΩ	E_e	117	Y_0	1.8×10^{-4}
C_p	1.023×10^{-8}	N	600	d_e	2.52×10^{-5}
F_n	0.10455	r_c	0.0052	d_m	0.005
M_t	0.0082	r_m	0.0042	b_s	0.01
m	0.0104	h_c	0.025	b_p	0.008
ρ_e	8960	h_m	0.020	b_e	0.0029
ρ_m	7400	h_s	0.00075	χ_n	9.6×10^{-5}
ρ_p	7800	h_p	0.00040	ζ_n	0.001
ρ_s	2700	d	0.001	φ_n	9.56×10^{-5}

The power outputs around the resonance frequency bandwidth for PE, EM, and ES methods have been exhibited in Figure 5.1. It is evident that the peak of the power occurs at resonance, i.e., the fundamental natural frequency ω_n which has been found 37.16 Hz by equation (22).

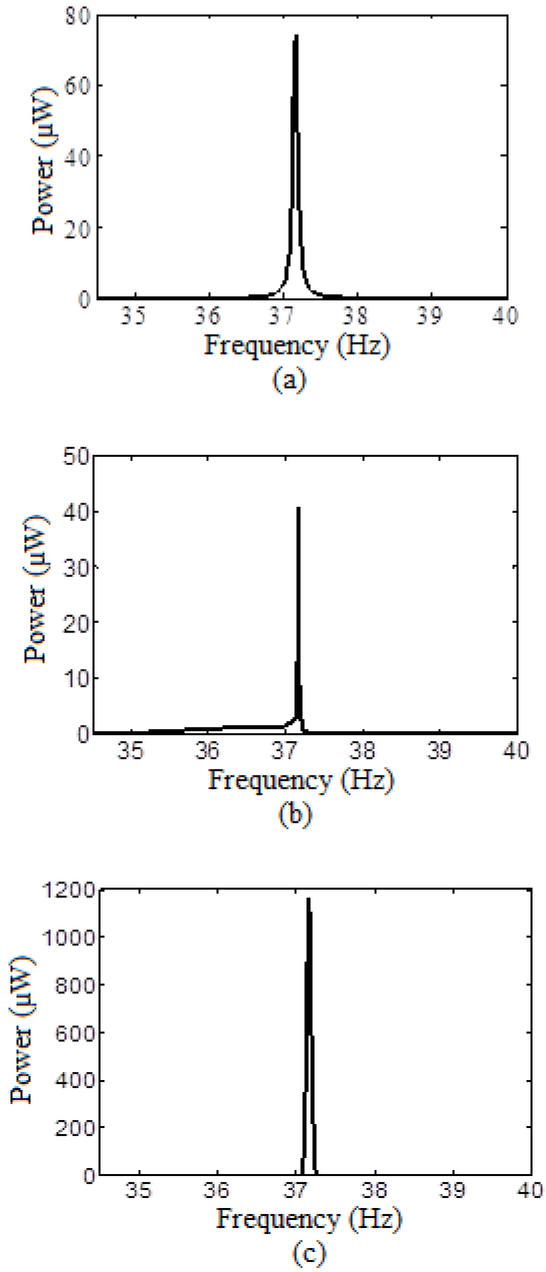

Figure 5.1: Power output of the three vibration-based standalone mechanisms at optimum load resistance: (a) PE, (b) EM, and (c) ES mechanism, respectively.

The optimal load resistance is determined as 200 kΩ based on the maximum power output of the PE mechanism at 37.16 Hz which is shown in Figure 5.2.

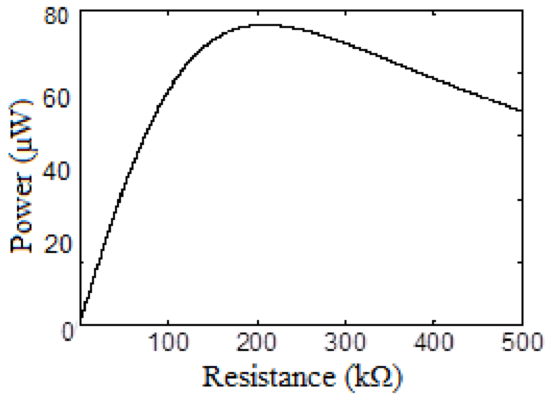

Figure 5.2: Determination of optimal load resistance R_L at the resonance with PE mechanism

5.2. Finite Element Analysis

5.2.1 Fundamental Frequency

To verify the value of ω_n, finite element analysis (FEA) in ANSYS Workbench 15.0 has been done which has resulted in 35.867 Hz with an error of 3.48% as compared to the analytical approach. It is notable that a lower resonant frequency as obtained from the current beam configuration is desirable; since it is close to the frequency of many physical vibration sources and opens up the opportunity to produce more power. That is why energy harvesters are generally designed to operate in the fundamental resonance frequency, i.e., the first mode of vibration which typically provides the maximum deflection and therefore gives the maximum electrical energy. Figure 5.3 (a) shows the first three normalized mode shape of a typical cantilever beam and Figure 5.3 (b) depicts the first resonant mode shape of the hybrid energy harvester. Both indicate good agreement on the mode shape. As mentioned in [27], the sign of the mode shapes of a cantilever beam during vibration is analogous to the sign of axial strain distribution along the length and any alteration in sign reduces the output voltage. Since, the first mode shape doesn't change its sign, the sign of the corresponding axial strain curve also remains unchanged, ensuring the generation of maximum voltage by the PZT layers. As a consequence,

strong emphasis has been given on the determination of fundamental resonance frequency and calculation of power and efficiency is also done based on that.

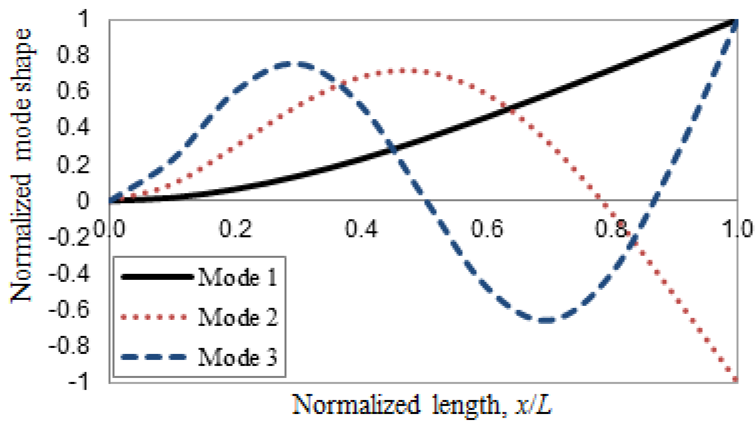

(a)

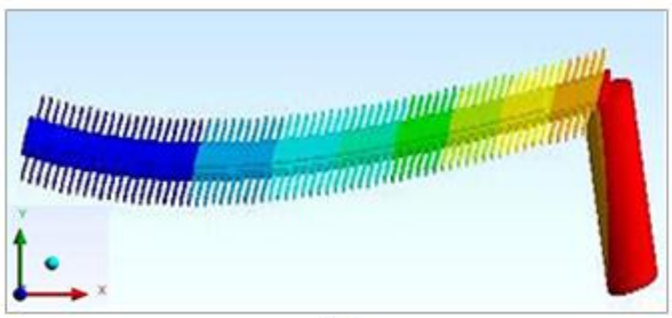

(b)

Figure 5.3: (a) First three mode shapes of a cantilever beam and (b) first mode shape of the hybrid beam obtained in FEA at ω_n= 35.866 Hz

5.2.1 Convergence Study

Based on the fundamental natural frequency, a mesh independence or, convergence study has been done in ANSYS where the value of ω_n converges to 35.867 Hz with the increase of degrees of freedom (DOF). Figure 5.4 represents the convergence study at the first mode shape corresponding to the converged ω_n value with the increase of DOF.

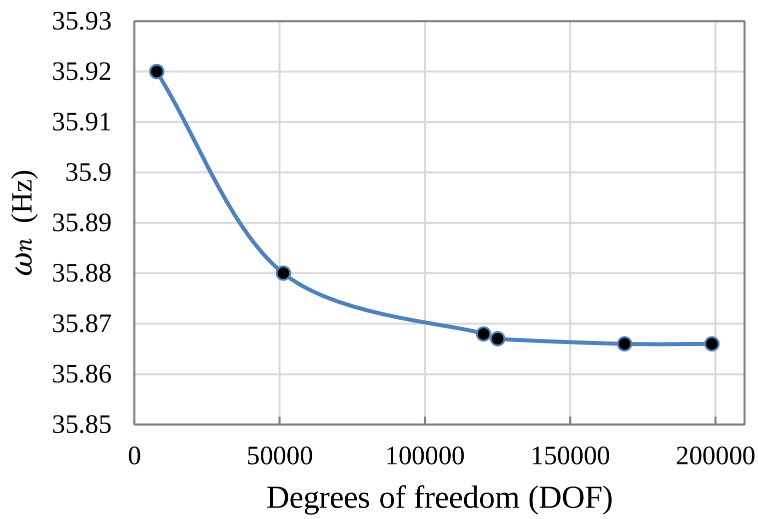

Figure 5.4: Convergence of ω_n with the increase of DOF

5.2.3 Fatigue Analysis

To study the failure criteria of the structure, fatigue analysis has also been done where the maximum principal stress on the beam has been found 2.93 MPa analytically with the equations given in the mathematical model. This indicates a fatigue life of at least 10^9 cycles as steered by the standard S-N curve for non-ferrous materials. It is remarkable that results in FEA for fatigue life also give the identical value (over 10^9 cycles) with a principal stress of 2.868 MPa which substantiates the agreement of the analytical calculation with the FEA solution. Figure 5.5 shows the distribution of the principal stress on the hybrid beam structure where the shear force at the free end is equal to the weight of the magnet. The maximum value of the principal stress corresponds to maximum tensile stress while the minimum value represents the maximum compressive stress.

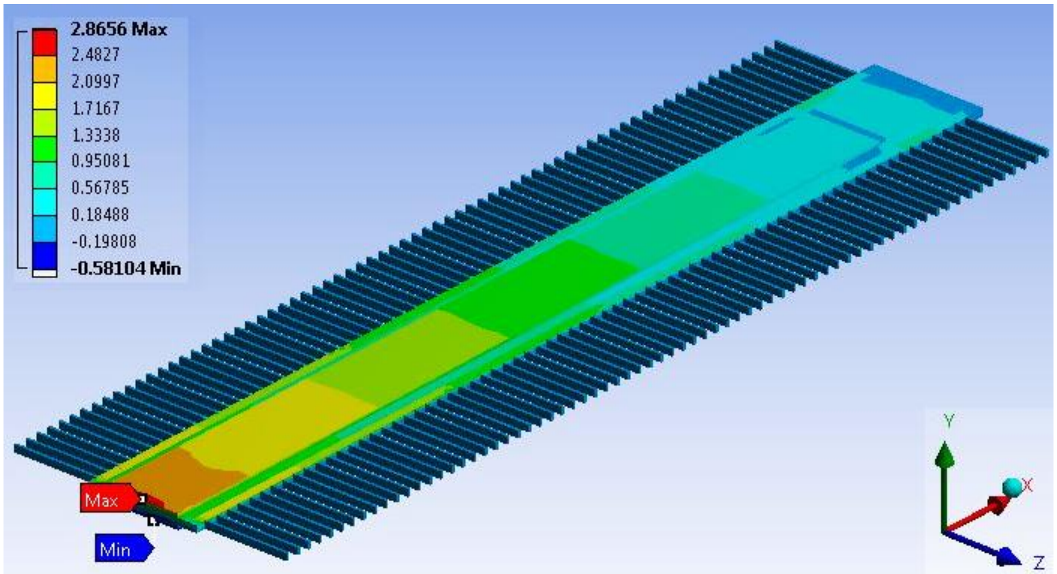

Figure 5.5: Distribution of principal stress on the hybrid beam due to fatigue loading

5.3. Calculation of Efficiency

The conversion efficiency of the hybrid energy harvester is determined by equation (34). The magnitude of P_{vib} is found 2193.701µW. On the other hand, the product of *irradiance* (132 mW/cm^2 at AM 1.5) and the effective PV cell area considering a total of eighty cells in four arrays yields the P_{solar} input as 105600 µW. The results for output power and efficiency are presented in Table 5.2.

Table 5.2: Results for power output and efficiency of the multifunctional energy harvester

Results	PV	PE	ES	EM	Hybrid	Hybrid (Vib)
Output Power (µW)	858.0	74.7	1164.6	40.5	2137.8	1279.8
Efficiency (%)	0.81	3.41	53.09	1.85	1.98	58.34

Results displayed in Figure 5.6 indicate that ES is the supreme contributor in the total output with an efficiency of 53.1%. PV generator is productive in terms of power output but less

efficient due to the massive input. With hybridization, an overall efficiency of 2% has been obtained which is greater than the efficiencies of PV and EM generators.

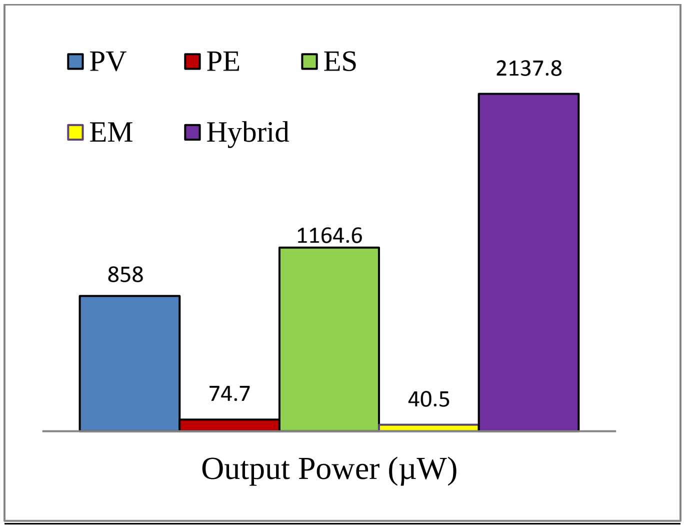

(a)

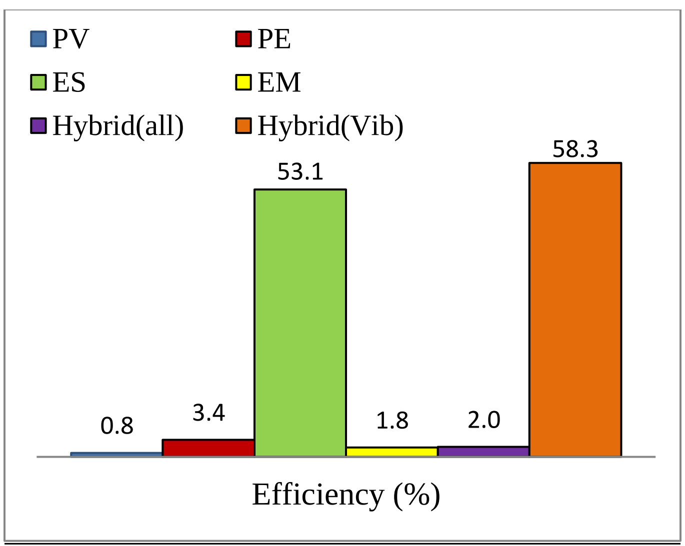

(b)

Figure 5.6: Column chart showing the results of (a) power output and (b) efficiency for standalone and hybrid mechanisms

It is conspicuous that, the hybrid vibration driven mechanism (without PV) outweighs all the stand-alone generators by constituting 58.3% efficiency. Still, PV is a tremendous boost-up

for any hybrid energy harvester as it supplies initial charge to ES capacitors and ominously upsurges the total power output.

5.4 Effect of Change in Scale of the Beam

The hybrid beam is assumed as the Euler-Bernoulli beam with a length of 100 mm in x direction, an effective width of 15.8 mm in z direction, and a thickness of 1.55 mm in y direction. Keeping the same width and thickness, if the length is scaled down to accommodate for small devices, the entire system will experience substantial changes in the performance, efficiency, and durability. It is obvious that power output will increase with the increase in size of the energy harvester. But, the size of the energy harvester module should be determined based on the possibility, application, and power requirement. Therefore, an appropriate scaling is incumbent to ripe the benefit from the energy harvester.

Since the fundamental natural frequency (ω_n) plays the most important role in the performance vibration-based energy harvesters, the effects of change in scale or size of the harvester on the fundamental natural frequency should be given the top priority. As the Expression for the ω_n suggests, the increase in length L will result in the decrease in the value of ω_n. A parametric study has been done with the proposed model to observe the effects of change in length and width on the natural frequency of the beam. Figure 5.7 and 5.8 show the results of the parametric study where it is clear that the changes in length and width have significant effects on the fundamental natural frequency of the beam. The value of ω_n decreases as the length of the beam increases. For a given input excitation, the decrease in natural frequency will essentially improve the performance of the energy harvester with the increase in power output. The values of the fundamental natural frequency at different lengths of the beam are presented in Table 5.3.

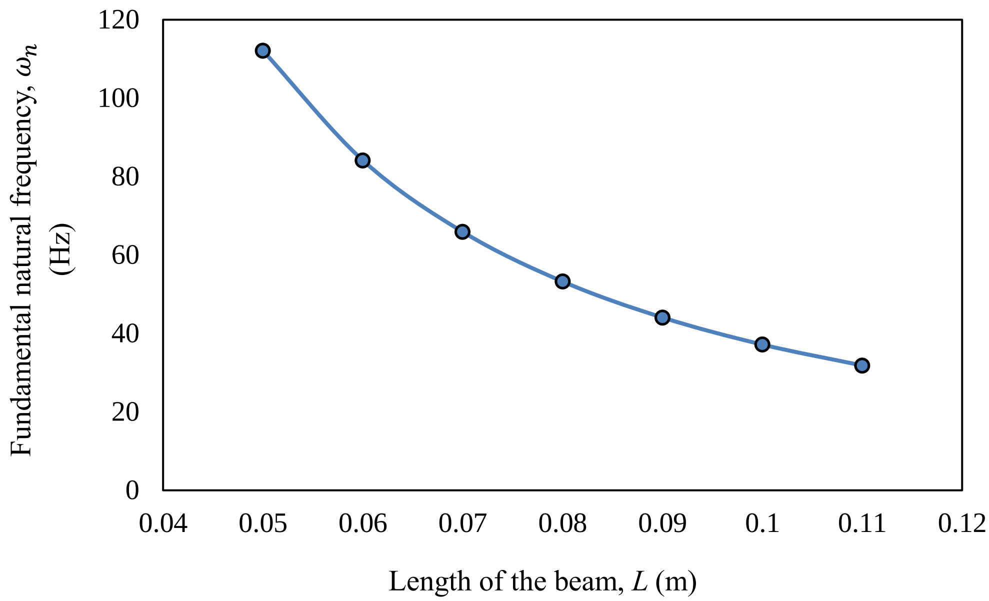

Figure 5.7: Effect of change in length on the fundamental natural frequency of the beam

Table 5.3: Variation in fundamental natural frequency with the change in length

Length, L (m)	ω_n (Hz)
0.11	31.834
0.10	37.1678
0.09	44.067
0.08	53.246
0.07	65.896
0.06	84.1429
0.05	112.119

On the other hand, if the widths of the substrate (b_s) and PZT layers (b_p) are increased, the increased width of the piezoelectric material will cause high forward modal coupling φ_n which will eventually increase the power output of the piezoelectric system. But, increasing width will decrease the length-width aspect ratio and therefore the beam may violate the Euler-Bernoulli beam theory. Therefore, in order to ignore the twisting of the beam by following Euler-

Bernoulli beam theory the width of the beam should be optimized. The aspect ratio of the beam for the proposed model has been considered 10:1 where the length is 100 mm and width of the Aluminum substrate is 10 mm. However, the width of the piezoelectric material should be equal or as much close to the substrate as possible in order to have more piezoelectric effect. But, in the proposed design the width of the PZT layers have been kept less than the width of the substrate in order to avoid contacts with the comb electrodes attached on two sides of the substrate.

The change in width of the beam will certainly have some effects on the fundamental natural frequency of the beam. For a given condition, it has been show in Figure 5.8 that the fundamental natural frequency increases as the width of the beam increases. Since higher natural frequencies are to be avoided, it is necessary to ensure the optimization of the geometry of the beam based on the fundamental natural frequency. The values of natural frequency at different widths of the beam are listed in Table 5.4.

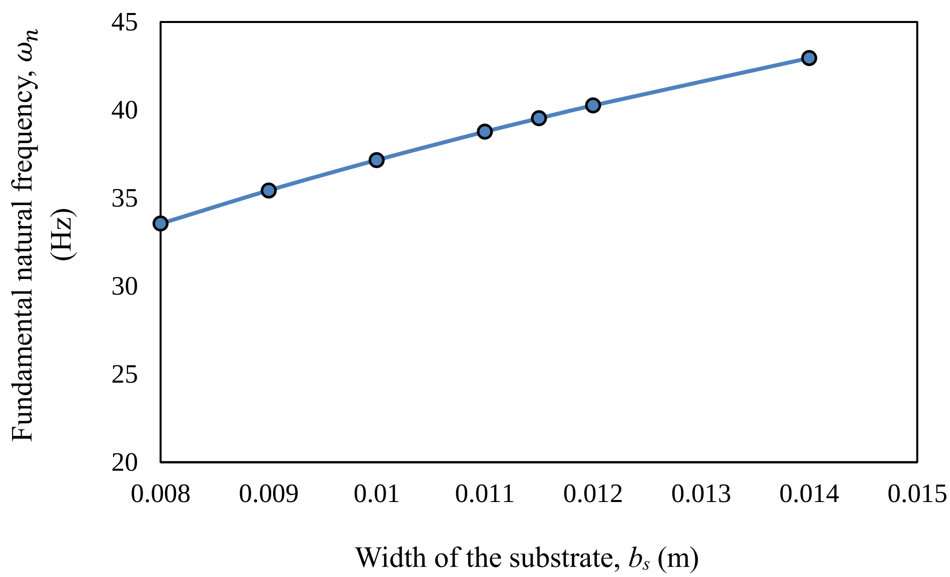

Figure 5.8: Effect of change in width on the fundamental natural frequency of the beam

Table 5.4: Variation in fundamental natural frequency with the change in width

Width of the substrate (m)	Width of a PZT layer (m)	ω_n (Hz)
0.008	0.006	33.547
0.009	0.007	35.435
0.01	0.008	37.164
0.011	0.009	38.769
0.0115	0.0095	39.526
0.012	0.010	40.257
0.014	0.012	42.952

6. Conclusions and Recommendations

6.1 Concluding Remarks

In this work, a self-energized multifunctional hybrid energy harvester has been investigated. Physical and mathematical model of the hybrid structure have been presented with illustrations. It has been shown that the hybrid device can generate more power than the stand alone generators with decent efficiency to replace the non-regenerative power sources. The initial power required to energize the variable capacitors is obtained by the photovoltaic technique. In absence of ambient illumination, the photovoltaic technique will not work which creates a constraint in the performance of the electrostatic converter. But, the power harvesting circuit is designed such that the electrostatic components can still obtain the initial bias input from the other mechanisms where failure of one generator will not result in disruption of the power generation. This allows a simultaneous conversion of energy and a continuous supply of power for the low-powered electronic components.

As the structure is subjected to transverse vibration, the cyclic loading or cyclic stress induced in the hybrid beam causes fatigue. Therefore, the fatigue analysis has been done for the weakest material, i.e., the Aluminum substrate and the expected life has been found quite reasonable comparing to the standard S-N curves. For a cantilever structure, the magnitude of stress should be the maximum near the fixed end and hence, it is much vulnerable to failure when subjected to cyclic loading. This is also verified by the finite element modeling results of the principal stress distribution on the hybrid beam in ANSYS Workbench 2015. The analytical results for the fundamental frequency, principal stress, and fatigue life show good agreement with the finite element analysis results.

Throughout the analysis, reciprocal interactions of the mechanisms have been ignored to avoid the complexity of the mechanisms. However, improvement can be done by considering a nonlinear system instead of a linear one. Deflection of the beam can be increased by applying change in geometries such as, using a triangular beam with gradually decreasing cross section towards the tip. Another way to significantly increase the power outputs from the energy harvester is to reduce the mechanical damping in the system. Besides, more than one magnet can be used to help generate more power in electromagnetic transduction. Again, Photovoltaic output can be obtained with decent efficiency using maximum power point tracking system. However, the theoretical and finite element model developed in this analysis facilitate the perception of hybrid energy harvesting technique, and escorts one to assimilate further versatility and robustness into such devices.

6.2 Recommendations and Future Work

Several modifications can be done in the modeling of the hybrid energy harvester in order to overcome the limitations of the power generation. The possible modifications and scope for future works are recommended below:

1. The geometry of the structure can be modified by considering a triangular shaped beam with gradual decrease in cross-section towards the tip. This implies a modification in the stiffness and damping formulae of the beam which opens another horizon of research based on the theory of elasticity.
2. In this analysis, the equation of motion of the cantilever beam is based on the assumptions of the Euler-Bernoulli beam theory considering no rotation or twisting (long beam with less thickness). Modifications can be done considering the Timoshenko beam theory or the theory of plates to incorporate the twisting effect into the displacement of

the beam and thus, investigate the natural frequencies and other parameters involved into the power generation calculation.

3. The photovoltaic (PV) panel considered in this device has area limitation due to the application in the fields of microelectromechanical systems and wireless sensor networks. Therefore, effective miniaturization of the PV panel along with maximum power point tracking technology can be a good option to upgrade its performance. This requires extensive study and experimental work which can be done in future.
4. Improvement on the electromagnetic (EM) transduction can be done by adding more magnets instead of only one and thereby associating multiple coils to generate more EM power. This can be quite beneficial as more magnets will also contribute to the total tip mass acting on the beam.
5. Since, the higher values of the modal coupling parameter (φ_n) in the Piezoelectric (PE) transduction ensures more PE power output, it is important to select proper materials and adjust the geometry such that φ_n becomes significant. For instance, possible techniques to increase the value of φ_n can be increasing the number of layers and width of the PE material, and so on. However, this requires a critical analysis of the parameters involved in it which offers further scope of research.
6. Throughout the analysis, the effect of one mechanism on the other was ignored. But, in practical cases there would be some effect on damping due to the attraction or repulsion of the magnetic and electric field. Investigating the reciprocal effects of these mechanisms on the power generation opens another scope to add new dimension in the analysis.

7. Results obtained by the theoretical analysis of the hybrid energy harvester have been compared with the finite element analysis (FEA) in ANSYS Workbench 15.0 which shows a decent agreement on finding the fundamental natural frequency and determining the fatigue criteria of the structure. Extensive work can be done using the software with versatile approaches in order to obtain more simulation results.
8. The linear energy harvester as proposed in this model has the limitation of operating in a narrow bandwidth. Maximum power output is obtained when the harvester operates at its fundamental natural frequency, which typically peaks over a very narrow range. However, frequency matching between the harvester and ambient vibrations can be difficult because of manufacturing tolerances, electric load changes, and excitation frequency changes as most sources do not have constant frequency spectrums.
9. The study on the cost-effectiveness of the hybrid energy harvester has not been done but, to implement such design into practical applications we need to calculate the cost of the material, fabrication, erection, and maintenance. This can also be done in future to determine the cost-effectiveness.
10. It is obvious that the study of the performance of the multifunctional hybrid energy harvester can be more acceptable and reliable if experimentation is done. Addition of some experimental results will certainly boost up the justification of the hybrid model.

REFERENCES

[1] Sodano H A, Inman D J, and Park G, 2004, "A Review of Power Harvesting from Vibration using Piezoelectric Materials," *The Shock and Vibration Digest*, **36**(3) 197–205.

[2] Ibrahim M, 2014, "Design, Modeling, and Fabrication of a Hybrid Energy Harvester," Master's thesis, University of Waterloo, Canada.

[3] Cook-Chennault K A, Thambi N, and Sastry A M, 2008, "Powering MEMS portable devices—a review of non-regenerative and regenerative power supply systems with emphasis on piezoelectric energy harvesting systems," *Smart Mater. Struct.* **17** 043001.

[4] Roundy S, 2003, "Energy scavenging for wireless sensor nodes with a focus on vibration to electricity conversion," *PhD* University of California, Berkeley.

[5] Collins L, 2006, "Harvesting for the world: energy harvesting techniques," *IEEE Power Eng*. **20** 34–7.

[6] Hamilton M C, 2012, "Recent advances in energy harvesting technology and techniques," *Proc. 38th Annu. Conf. IEEE Ind. Electron. Soc.,*Montreal, QC, Canada, 6297−304.

[7] Davidson J and Mo C, 2014, "Recent advances in energy harvesting technologies for structural health monitoring applications," *Smart Mater. Res.* **2014** 410316.

[8] S. Priya and D.J. Inman, *Energy Harvesting Technologies* [Electronic Resource], Springer, New York, 2008.

[9] Park G, Rosing T, Todd M, Farrar C, and Hodgkiss W, 2008, "Energy harvesting for structural health monitoring sensor networks," *Journal of Infrastructure Systems*, **14** 64–79.

[10] Roundy S, Leland E S, Baker J, Carleton E, Reilly E, Lai E, Otis B, Rabaey J M, Wright P K, and Sundararajan V, 2005, "Improving power output for vibration-based energy scavengers," *IEEE Pervasive Comput.* **4** 28–36.

[11] Miles R W, Hynes K M, and Forbes I, 2005, "Photovoltaic solar cells: an overview of state-of-the-art cell development and environmental issues," *Prog. Cryst. Growth Charact. Mater*. **51** 1–42.

[12] L.D. Partain (Ed.), *Solar Cells and Their Applications*, Wiley, 1995.

[13] M.A. Green, *Solar Cells: Operating Principles, Technology and Systems Applications*, Prentice-Hall, 1992.

[14] Lee J B, Chen Z Z, Allen M G, Rohatgi A, and, Arya R, 1995, A miniaturized high-voltage solar-cell array as an electrostatic mems power-supply *J. Microelectromech. Syst.* **4** 102–108.
[15] Sakakibara T, Izua H, Shibata T, Tarui H, Shibata K, Kiyama S, and Kawahara N, 2002, "Multi-source power supply system using micro-photovoltaic devices combined with microwave antenna," *Sensors Actuators* A, **95** 208–11.
[16] Lewis J, Zhang J, and Jiang X, 2009, "Fabrication of organic solar array for applications in micro-electromechanical systems," *J. Renewable Sustainable Energy* **1** 013101.
[17] Sample A and Smith J R, 2009, "Experimental results with two wireless power transfer systems," *IEEE Radio and Wireless Symp.* San Diego, CA, USA, 16–8.
[18] Strasser M, Aigner R, Franosch M, and Wachutka G, 2002, "Miniaturized thermoelectric generators based on poly-Si and poly-SiGe surface micromachining," *Sensors Actuators A,* **97** 535–42.
[19] Lawreence E E and Snyder G J, 2002, "A Study of Heat Sink Performance in Air and Soil for Use in a Thermoelectric Energy Harvesting Device," *Proc. 21st Int. Conf. Thermoelec.*, Portland, OR, 446–449.
[20] Starner T, 2005, "*Low-Power Electronics Design*," Boca Raton: CRC Press, ch 45.
[21] Wu W, Bai S, Yuan M, Qin Y, Wang Z L, and Jing T, 2012, "Lead zirconate titanate nanowire textile nanogenerator for wearable energyharvesting and selfpowered devices," ACS Nano, **6** 6231–5
[22] Qi Y, Jafferis N T, Lyons Jr K, Lee C M, Ahmad H, and McAlpine M C, 2010, "Piezoelectric ribbons printed onto rubber for flexible energy conversion," *Nano Lett*., **10** 524–8.
[23] Chang C, Tran V H, Wang J, Fuh KY and Lin L, 2010, "Directwrite piezoelectric polymeric nanogenerator with high energy conversion efficiency," *Nano Lett*., **10** 726–31.
[24] Yang R, Qin Y, Li C, Zhu G, and Wang Z L, 2009, "Converting biomechanical energy into electricity by a musclemovementdriven nanogenerator," *Nano Lett*., **9** 1201–5.
[25] Anton S R and Sodano H A, 2007, "A review of power harvesting using piezoelectric materials (2003–2006)," *Smart Mater. Struct.* **16** R1–21.
[26] Zhang Y, 2014, "Piezoelectric based energy harvesting on low frequency vibrations of civil infrastructures" *PhD* Lousiana State University, Baton Rouge, LA.
[27] Erturk A, 2009, "Electromechanical Modeling of Piezoelectric Energy Harvesters" PhD Virginia Polytechnic Institute and State University, Blacksburg, VA.

[28] Erturk A and Inman D J, 2009, “An experimentally validated bimorph cantilever model for piezoelectric energy harvesting from base excitations,” *Smart Mater. Struct.* **18** 025009.
[29] Erturk A and Inman D J, 2008, “On mechanical modeling of cantilevered piezoelectric vibration energy harvesters,” *J. Intell. Mater. Syst. Struct.* **19** 1311–25.
[30] D. P. Arnold, 2007, “Review of microscale magnetic power generation,” *IEEE Trans. Magn.* **43**, 3940–3951.
[31] Williams C B and Yates R B, 1996, “Analysis of a Micro-electric Generator for Microsystems,” *Sensors and Actuators A*, **52** 8–11.
[32] Glynne-Jones P, Tudor M J, Beeby S P, and White N M, 2004, “An Electromagnetic, Vibration-powered Generator for Intelligent Sensor Systems,” *Sensors and Actuators A*, **110** 344−349.
[33] Beeby S P, Tudor M J, and White N M, 2006, “Energy harvesting vibration sources for microsystems applications,” *Meas. Sci. Technol.* **13** R175–95.
[34] Mitcheson, P., Miao, P., Start, B., Yeatman, E., Holmes, A. and Green, T., 2004, “MEMS Electrostatic Micro-Power Generator for Low Frequency Operation,” Sensors and Actuators A, **115** 523-529.
[35] Roundy, S., Wright, P. and Rabaey, J., 2003, “*Energy Scavenging for Wireless Sensor Networks*,” Kluwer Academic Publishers, Boston.
[36] Boisseau S, Despesse G, Ricart T, Defay E and Sylvestre A, 2011, “Cantilever-based electret energy harvesters,” *Smart Mater. Struct.*, **20** 105013.
[37] Tao K, Miao J, Lye S, and Hu X, 2015, “Sandwich-structured Two-dimensional MEMS Electret Power Generator for Low-level Ambient Vibrational Energy Harvesting,” *Sensors and Actuators A: Physical*, **228** 95–103.
[38] Wang L, 2007, “Vibration energy harvesting by magnetostrictive material for powering wireless sensors,” *PhD* North Carolina State University, Raleigh.
[39] Zhang H, 2011, “Power generation transducer from magnetostrictive materials,” *Appl. Phys. Lett.*, **98** (23) 232505.
[40] C.Natale, C.Visone, e F. Velardi, , 2001, “Identification and compensation of Preisach hysteresis models for magnetostrictive actuators,” *Physica B*, **306** 161–165.

[41] Shan X B, Guan S W, Liu Z S, Xu Z L, and Xie T, 2013, “A new energy harvester using a piezoelectric and suspension electromagnetic mechanism,” *J Zhejiang Univ-Sci A (Appl. Phys. & Eng.)* **14**(12) 890−897.
[42] Larkin M and Tadesse Y, 2013, “HM-EH-RT: hybrid multimodal energy harvesting from rotational and translational motions,” *Int. J. Smart and Nano Materials*, **4** 257– 285.
[43] Challa V R, Prasad M G, and Fisher F T, 2009, “A coupled piezoelectric–electromagnetic energy harvesting technique for achieving increased power output through damping matching,” *Smart Mater. Struct*., **18** 005029.
[44] Khaligh A, Zeng P, and C. Zheng, 2010, “Kinetic energy harvesting using piezoelectric and electromagnetic technologies—State of the art,” *IEEE Trans. Ind. Electron*., **57** 850–60.
[45] Yang B, Lee C, Kee L W, and Lim P S, 2010, “Hybrid energy harvester based on piezoelectric and electromagnetic mechanisms,” *J. Micro/Nanolith. MEMS MOEMS,* **9** 023002.
[46] Khbeis M, McGee J, Richardson C, and Ghodssi R, 2006, “Design of hybrid ambient low frequency, low intensity vibration energy scavenger,” *Proc. PowerMEMS*, Berkeley, California, 287−90.
[47] Khbeis M, McGee J, Ghodssi R, 2009, “Development of a Simplified Hybrid Ambient Low Frequency Low Intensity Vibration Energy Scavenger System,” *Transducers 2009,* Denver, CO, 525−528.
[48] Eun Y, Kwon D, Kim M, Yoo I, Sim J, Ko H, Cho K, and Kim J, 2014, “A flexible hybrid strain energy harvester using piezoelectric and electrostatic conversion,” *Smart Mater. Struct*., **23** 045040.
[49] Gambier P, Anton S R, Kong N, Erturk A, and Inman D J, 2012, “Piezoelectric, solar and thermal energy harvesting for hybrid low-power generator systems with thin-film batteries,” *Meas. Sci. Technol*., **23** 01510.
[50] Goudarzi M, Niazi K, and Besharati M K, 2013, “Hybrid energy harvesting from vibration and temperature gradient by PZT and PMN-0.25PT ceramics,” *Mater. Phys. Mech.*, **16** 55– 65.
[51] Yu H, Yue Q, Zhou J, and Wang W, 2014, “A hybrid indoor ambient light and vibration energy harvester for wireless sensor nodes,” *Sensors,* **14** 8740−55.
[52] Colomer-Farrarons J, Miribel-Catala P, Saiz-Vela A, and Samitier J, 2011, "A Multiharvested Self:Powered System in a Low-Voltage Low-Power Technology," *IEEE Trans. Ind. Electron*., **58**(9) 4250−63.

[53] http://www.acoustical-consultants.com/noise-vibration-acoustical-related-resources
[54] Baker J, Roundy S, and Wright P, 2005, "Alternative Geometries for Increasing Power Density in Vibration Energy Scavenging for Wireless Sensor Networks," *Proc. 2005 3rd Int. Energy Conversion Engineering Conf.,* **8** 1−12.
[55] Chen Z S, Yang Y M, and Deng G Q, 2009, "Analytical and experimental study on vibration energy harvesting behaviors of piezoelectric cantilevers with different geometries," *Int. Conf. on Sustainable Power Generation and Supply*, Nanjing, China: IEEE, 1–6.
[56] Challa V R, Prasad M G, Shi Y, and Fisher F T, 2008, "A vibration energy harvesting device with bidirectional resonance frequency tenability," *Smart Mater. Struct*., **17** 015035.
[57] https://www.coursehero.com/file/12001850/S-N-diagram/
[58] Sood V K and Bhalla P, 2013, "EMTP Model of Grid Connected PV System," Proc. Int. Conf. on Power System Transients, Vancouver, Canada, 1−8.
[59] Yi J W, Shih W Y, and Shih W H, 2002, "Effect of length, width, and mode on the mass detection sensitivity of piezoelectric unimorph cantilevers," *J. Appl. Phys,.* **91** 1680-6.
[60] Cottone F, 2011, "Introduction to vibration energy harvesting," *NiPS Energy Harvesting Summer School.*
[61] Kim J, Cottone F, Goyal S, and Punch J, 2010, "Energy scavenging for energy efficiency in networks and applications," *Bell Labs Tech. J.,* **15** 7–29.
[62] Anderson T A and Sexton D W, 2006, "A Vibration Energy Harvesting Sensor Platform for Increased Industrial Efficiency," *Proc. of the SPIE,* **6174** 621−629.
[63] Challa V R, Prasad M G, and Fisher F T, 2011, "Towards an autonomous self-tuning vibration energy harvesting device for wireless sensor network applications," *Smart Mater. Struct*., **20** 025004.
[64] Bermejo S, Ortega P, Jimenez J J and Castaner L, 2005, Response of c-Si PV arrays under monochromatic light for MEMS power supply *J. Micromech. Microeng.,* **15** 1446–53.
[65] Wang Q M and Cross L E, 1999, "Constitutive Equations of Symmetrical Triple Layer Piezoelectric Benders," *IEEE Transactions on Ultrasonics, Ferroelectrics, and Frequency Control,* **46** 1343–1351.

VITA

The author was born in the city of Brahmanbaria, Bangladesh and passed his early school and college years in Dhaka, the capital of Bangladesh. He obtained his Bachelor's degree in Mechanical Engineering in 2011 from the Islamic University of Technology, a subsidiary organ of OIC (Organization of Islamic Cooperation). After graduation, he joined the People's University of Bangladesh, Dhaka, Bangladesh and served there up to May 2012 as a Lecturer in Mechanical Engineering. Then he joined Primeasia University in the Textile Engineering Department in June 2012 and worked as a lecturer for over two years before coming to USA. In the Fall 2014, he joined the University of New Orleans to pursue his Ph.D. in Engineering and Applied Science and continuing there up to now.